Thesis for doctoral degree (Ph.D.)
2020

MRI SEQUENCES FOR DETECTION OF ACUTE PULMONARY EMBOLISM

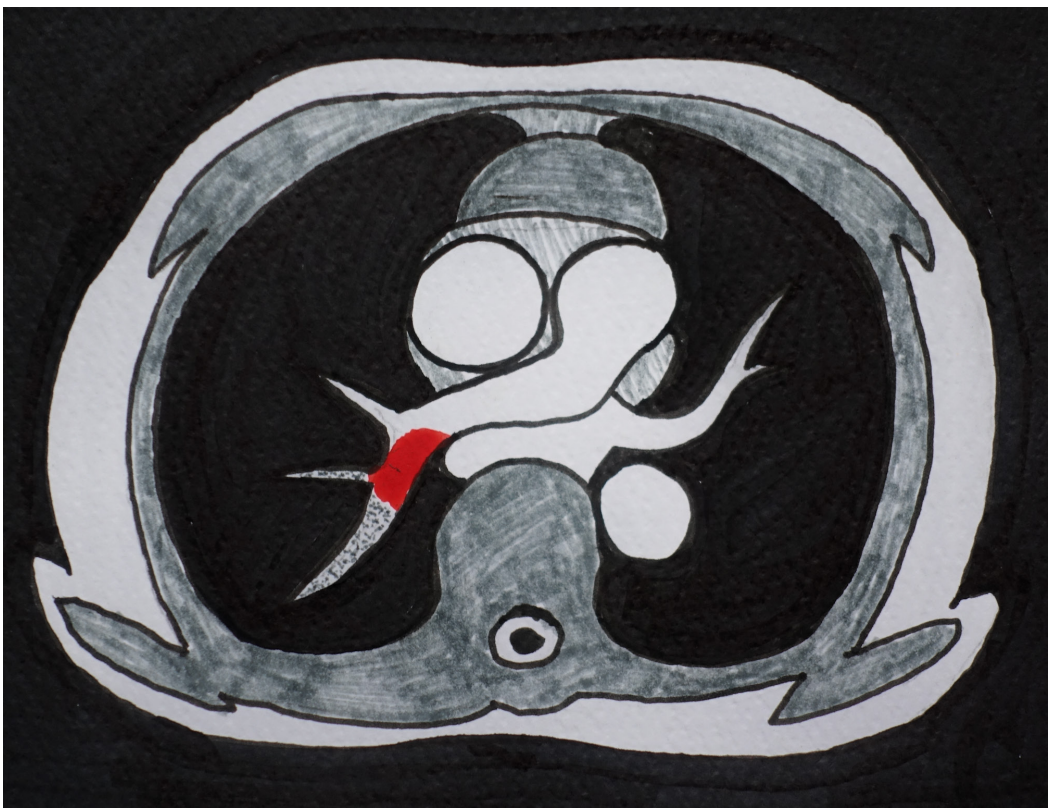

Roberto Vargas Paris

Karolinska Institutet

From the Department of Physiology and Pharmacology
Karolinska Institutet, Stockholm, Sweden

MRI SEQUENCES FOR DETECTION OF ACUTE PULMONARY EMBOLISM

Roberto Vargas Paris

Karolinska Institutet

Stockholm 2020

Published by Karolinska Institutet.
Printed by Universitetsservice US-AB, 2020

ISBN 978-91-7831-976-3
Cover illustration: by Veli Söderlund

MRI sequences for detection of acute pulmonary embolism
THESIS FOR Doctoral degree (PhD)

By

Roberto Vargas Paris

The thesis will be defended in public at Karolinska University Hospital, Eugeniavägen 3, Stockholm, Solna, J3:14, Onsdag den 16 December 2020, kl 09:00

Principal Supervisor:
Associate Professor Peter Lindholm
Karolinska Institutet
Department of Physiology and Pharmacology

Co-supervisor(s):
Associate Professor Sven Nyrén
Karolinska Institutet
Department of Molecular Medicine and Surgery
Division of Diagnostic Radiology

MD PhD Mikael Skorpil
Karolinska Institutet
Department of Molecular Medicine and Surgery
Division of Neuroradiology

Opponent:
Professor Tino Ebbers
Linköping University
Department of Medicine and Care
Division of Cardiovascular Medicine

Examination Board:
Associate Professor Nikolaos Kartalis
Karolinska Institutet
Department of Klinisk Vetenskap, Intervention och Teknik
Division of Diagnostic Radiology

Associate Professor Anna Ågren
Karolinska Institutet
Department of Molecular Medicine and Surgery, and Department of Science, Danderyds Hospital
Division of Coagulation Centrum

Associate Professor Erik Hedström
Lunds University
Department of Clinical Physiology
Division of Diagnostic Radiology

Para mi hijas, nietas (os), mi madre, padre, para toda mi querida familia, les dedico este trabajo con amor, dedicacion y erfuerzo.

The more I learn, the more time I have for my patients,……..
Roberto Vargas Paris

POPULAR SCIENCE SUMMARY OF THE THESIS

Pulmonary embolism (PE) is caused by blockage of the pulmonary arteries and is a life-threatening condition; it can be caused a range of diseases, or due to the patient's circumstances, for example if they are hospitalized and bed-ridden, or as a result of surgery. The condition is caused by the body forming a clot or clots, often in the legs, which then occludes or stops the normal blood circulations in the veins. If the clot detaches from the legs and enters the circulation, it may then travel up through the major veins to the heart. From there, the journey continues towards the pulmonary arteries. The pulmonary arteries become increasingly smaller in diameter as the clot travels into the lungs, until it reaches a point at which the clot is too large to travel any further. The clot then plugs the artery and stops the blood flow in that part of the lung tissue. If the clot remains, then the tissue will not be oxygenated. The process of blood oxygenation in the lungs may also decrease, reducing or affecting delivery of oxygenated blood to the whole body. Pulmonary embolism is a serious and acute condition, which should be investigated and treated as soon as possible to avoid mortality.

In an emergency, PE is often difficult to diagnose; patients may present with various signs and symptoms that are non-specific to the disease, such as chest pain, cough, and heavy or irregular breathing for example. Blood tests and other diagnostics can help, but in this situation pulmonary imaging is of most use to the physician. Generally, a computed tomography (CT) scan is employed to diagnose a suspected PE. This imaging method requires contrast medium to be injected into the bloodstream of the patient and for most, this is relatively harmless. However, some patients are contraindicated for the contrast media, due to impaired kidney function or allergic sensitivity, making a CT scan impossible for this cohort.

In this thesis, a range of methodologies that use magnetic resonance camera technology to investigate the presence of blood clots is considered. Magnetic resonance imaging (MRI), unlike the CT scanning technique, does not require contrast media injection in order to visualize blockages in the vessels. Therefore, the technique is well suited to patients who are hypersensitive or whose kidneys will not tolerate the injection of contrast agents. In MR images, the blood appears white, while the plug or clot will be gray, and so differentiation between the two may be made. During the process of imaging the pulmonary region, patients may also be asked to hold their breath to reduce any movement artefact in the image. Many patients find this difficult to achieve, and so as another aspect of this thesis, we also tested MRI techniques whereby breath holding was not necessary.

POPULÄRVETENSKAPLIG SAMMANFATTNING

Lungembolism är ett sjukdomstillstånd där det fastnar blodproppar i lungkärlen. Det kan orsakas av olika sjukdomar eller tillstånd som ökar blodets förmåga att koagulera (bilda blodproppar). Dessutom ökas risken av stillasittande som ex flygresor, vara sängliggande en lång period eller att genomgå en operation. Dessa är exempel som gör en risk att kroppen bildar en propp eller proppar i en ven, ofta längst ner i benen. En propp är en klump av blod. Denna propp ockluderar eller stoppar blodströmmen i venerna, tillbaka till hjärta och lungor.

Ibland händer att denna proppen lossnar och med hjälp av det cirkulerande blodet, och transporteras upp genom de stora kroppvenerna till hjärta. Därifrån fortsätter resan mot lungkärlet. Såsom lungkärlet eller lungartär blir mindre och mindre desto mer proppen flyttas in i lungan, tills den når en vis position där proppen kommer inte att komma vidare på grund av sin egen storlek i relation till kärlets storlek. Då stannar proppen, där namnet propp, och orsakar att blodet inte når fram eller sker en minskning av det normala blodflödet till en vis del av lungvävnaden. Denna vävnad som inte få blod kan död av näringsbrist. Dessutom minskar möjligheten att syresätta blodet i lungorna, delvis beroende på propens storlek. Det orsakar ett allvarligt och akut patienttillstånd, som bör utredas och behandlas snarast.

Akutläkare har många gånger svårt att ställa diagnosen lungemboli eller propp i lungkärlet. Detta ofta på grund av patienterna har olika tecken som kan vara ospecifika för sjukdom, tex ont i bröstet eller bröstkorgen, hosta, svår eller oregelbunden andning, osv. Blodprov och andra tester kan hjälpa till. Men väldigt ofta beställer man bilder av lungkärlen. Den mest användbara och vanligaste testet är skiktröntgen (datortomografi). Denna bildmetod använder röntgenstrålning och har behov av spruta kontrastmedel in i blodet. För de flesta patienter fungerar väldig bra och är relativ ofarligt. Det finns en del patienter som på grund av nedsatt njurfunktion eller allergisk känslighet, inte kan få detta kontrastmedel, och då kan man ej göra skiktröntgen.

I denna avhandling vill vi presentera en metod som använder magnetkamerateknik, inte skiktröntgen, för att avbilda de proppar som kan finnas i lungkärlen. Denna metod behöver inte injektionen av kontrastmedel i blodet. Denna teknik passar bra för den patientgrupp som är överkänslig eller vars njurar inte tål kontrastmedel. Patienterna behöver inte heller hjälpa till med att hålla andan under bildtagningen utan kan andas fritt helat tiden. Vi har testat olika sätt att göra bilder med magnetkameran, med fokus på nya metoder att samla i data, som ska vara mindre känslig för patientens rörelse, som andningen: Vi har också gjort möjligt att bearbeta data för att skapa ”snabba bilder” med bättre kvalitet. Vi kan framställa eller visa blodet och proppen på olika sett i bilderna, som hjälper till att identifiera om det finns ett stopp i lungkärlets blodflöde.

ABSTRACT

In recent years a range of imaging techniques have emerged to help diagnose patients with suspected acute Pulmonary Embolism (PE). This is particularly useful for those who are contraindicated (renal failure or allergies) to the contrast media that is needed to perform Computed Tomography Pulmonary Angiography (CTPA), which would be the usual diagnostic tool of choice. To aid the cohort of patients with this contraindication, we have investigated the option of using Magnetic Resonance Imaging (MRI) to diagnose PE. In this thesis, MRI sequences including gradient recall echo (more specifically balanced Steady State Free Precession [b-SSFP]) with different trajectories of data sampling, and diffusion weighted imaging (DWI) were assessed. None of the sequences investigated required the use of intravenous contrast media.

In Study I, we investigated a group of positive PE patients (verified by CTPA) alongside a volunteer group, who provided a negative PE control cohort. A b-SSFP sequence was assessed, using repetitive sampling of each slice position, in three different orthogonal planes. No triggering or breath hold techniques were used during imaging. This technique produced a large number of slices at each location for evaluation by radiologist. An excellent specificity and a good sensitivity were achieved.

In Study II, a group of positive PE patients (also verified by CTPA) and a control volunteer group were used to test the DWI technique, which is not used commonly for the investigation of thrombosis in the lungs. We compared DWI against the single slice per position approach of b-SSFP and CTPA, and demonstrated its capability to depict pulmonary embolism, finding a very high sensitivity but poor specificity for DWI.

In Study III, we tested two different sampling techniques for b-SSFP, Cartesian standard and golden angle radial sampling trajectories, to image the pulmonary arteries in ten volunteers and in two patients who had PE. We demonstrated the improvement of image quality when using radial trajectory sampling in comparison to the Cartesian technique. We also demonstrated that the post-reconstruction ‘sliding window’ method could be applied to the golden angle radial sampling schema when a different temporal resolution is needed.

In Study IV, we used the sequence tested in Study III (b-SSFP with golden angle radial and Cartesian sampling) in a clinical setting. The study included 64 patients who were suspected of having acute PE; all were examined while waiting for CTPA diagnostic testing. We compared radial sampling versus Cartesian, and also assessed post-reconstruction images of the radial sampling, with varying temporal resolution. The radial sampling with golden angle schema did not produce images of high enough quality to depict acute PE in patients.

In study V, a retrospective overview of 57 patients (2012–2018) from our institution, with suspected acute PE was made. This group of patients was contraindicated to CTPA, and so were examined only using b-SSFP images. The clinical outcome of this cohort was obtained from the electronical medical record system up to twelve months after their MRI assessments. The MRI results allowed the clinicians to change or support their decision as to which treatment strategy they chose, in patients with or without PE.

LIST OF SCIENTIFIC PAPERS

I. Detection of pulmonary embolism using repeated MRI acquisitions without respiratory gating: a preliminary study*.
Nyrén S., Nordgren Rogberg A., **Vargas Paris R**., Bengtsson B., Westerlund E., Lindholm P.
Acta Radiol. 2017 Mar; 58(3): 272-278

II. Diffusion-weighted imaging in acute pulmonary embolism: a feasibility study.
Vargas Paris R., Skorpil M., Westerlund E., Lindholm P., Nyrén S.
Acta Radiol Open. 2018 Jun; 7(6): 2058460118783013

III. Pulmonary artery imaging under free-breathing using golden-angle radial bSSFP MRI: a proof of concept.
Fyrdahl A., **Vargas Paris R**., Nyrén S., Holst K., Ugander M., Lindholm P., Sigfridsson A.
Magn Reson Med. 2018 Nov; 80(5):1847-56

IV. Clinical evaluation of radial golden angle b-SSFP with sliding window MRI for detection of acute pulmonary embolism.
Vargas Paris R., Fyrdahl A., Medson K., Yu J., Skorpil M., Nyrén S., Sigfridsson A., Lindholm P.
Manuscript 2020.

V. Primary diagnosis of pulmonary embolism with unenhanced MRI for patients not eligible for CTPA: Clinical outcome.
Medson K., **Vargas Paris R**., Nordgren Rogberg A., Sigbergsdottir A., Nyrén S., Lindholm P.
Eur J Radiol Open. 2019;6:315-319

*Awarded by *Xenia Fosselliana Prize 2017* as the best scientific article from a Nordic institution published in Acta Radiologica 2017.

CONTENTS

LIST OF ABBREVIATIONS

2D	two dimensional
3D	three dimensional
ADC	Apparent diffusion coefficient
ASSET	Array spatial sensitivity encoding technique
ASL	Arterial spin labeling
Balanced FFE	Balanced fast field echo
b-SSFP	Balanced steady state free precession
CNR	Contrast to noise ratio
CTPA	Computed tomography pulmonary angiography
DVT	Deep vein thrombosis
DWI	Diffusion weighted imaging
ECG	Electrocardiogram
FIESTA	Fast imaging employing steady state acquisition
FLASH	Fast low angle shot
FOV	Field of view
Gd	Gadolinium
GFR	Glomerular filtration rate
GRAPPA	Generalized auto-calibrating partially parallel imaging
GRE	Gradient recall echo
IPat	Integrated parallel acquisition technique
MRA	Magnetic resonance angiography
MRI	Magnetic resonance imaging
NSF	Nephrogenic system fibrosis
PE	Pulmonary embolism
PIOPED	Prospective investigation of pulmonary embolism diagnosis
PROPELLER	Periodically rotated overlapping Parallel lines with enhanced reconstruction
SENSE	Sensitivity encoding
SNR	Signal to noise ratio
SPECT	Single photon emission computed tomography

TE	Time of echo
TOF	Time of flight
TR	Time of repetition
True-FISP	True fast imaging with steady state precession
VTE	Venous thromboembolism
V/Q	Ventilation and perfusion scintigraphy

1 INTRODUCTION

Within the human body, an equilibrium exists between two different processes, thrombosis and fibrinolysis. Thrombosis is the process of the formation of a blood clot in the circulation, while the anticlotting process, fibrinolysis, occurs to dissolve the clot. The balance between the two processes is constant; its disruption does not always cause morbidity; however, it can cause the formation of stationary or itinerant blood clots in the circulation (1,2).

Venus thromboembolism (VTE) is a condition whereby blood clots (thrombi) form, most often in the deep veins (deep vein thrombosis; DVT) causing morbidity. When such clots build in the distal veins then travel through the venous system to the pulmonary circulation, they may initiate a reduction in blood flow in the pulmonary arteries causing a perfusion defect, and a pulmonary embolism (PE) occurs (3).

Stroke, cardiac infarction and PE are the three most common cardiovascular diseases. Many authors have acknowledged the potentially fatal outcome from PE. Studies have shown a mortality of between 10% to 30% within a month of having VTE, and most of these present with a PE (3). When PE is associated with cancer and/or cardiovascular disorders then an outcome of death within a year is not rare.

Robust and effective diagnostic tools are necessary to determine the presence of PE and allow the most effective treatment to be administered; this is essential to reduce morbidity and mortality. From the time of the first Prospective Investigation of Pulmonary Embolism Diagnose (PIOPED) study in 1990 to recent years, there have been many attempts to find the most effective imaging tool to help clinicians in the diagnosis of patients suffering from cardiovascular disease, especially PE. The Computed Tomography Pulmonary Angiography (CTPA) technique is the method most often used today. However, it may be contraindicated by renal failure or allergies to the intravenous contrast media for example, and so there is a unmet need for alternative techniques, especially when using magnetic resonance imaging (MRI).

2 LITERATURE REVIEW

2.1 BACKGROUND

Within the group of cardiovascular diseases, PE is the third most common cause of death, after stroke and heart infarction. Two thirds of patients with VTE also have DVT; one third of these present with PE, and this condition represents a high risk of mortality for VTE patients (3). At least 59% of all cases of VTE occur in inpatients. For those patients with cancer, ongoing surgical procedures, immobility, and trauma there is an increasing correlation or a higher risk factor for developing VTE (4,5). Given that hospitalization with or without surgery represents 24% and 22% of VTE cases respectively, the roll of a prophylaxis for these patients is crucial (4,5).

The consequences of PE going undiagnosed and untreated can be severe, with up to 30% mortality rates (6). In a group of around 400 patients diagnosed with PE, 95 died within one year due to related cancer, sepsis and cardiac disease, while 10.5% died directly from PE. The size of the thrombotic process has a huge impact on clinical outcome and also affects the ability to image and then diagnose PE accurately. Autopsies primarily check the major vessels; smaller vessels are rarely investigated, and this discrepancy could explain the wide variance in autopsy results with regards to PE (1.5% to 30%) (7). In a random series of 508 autopsies, the prevalence of PE was 70% but 20% were identified in a microscopic examination (1), (8).

Often the symptoms of PE are not specific and are seemingly unrelated to the illness itself. Many patients present with symptoms such as chest pain, dyspnea, tachycardia, hypotension, cough, and hemoptysis (9). The diagnosis and treatment protocol for patients with suspected PE involves a mix of clinical scoring systems, such as that developed by Wells (10) or the Geneva scoring system, serum testing, electrocardiogram (ECG) and varying imaging modalities, including chest X-ray, computed tomography pulmonary angiography (CTPA), ventilation and perfusion scintigraphy (V/Q) and magnetic resonance imaging (MRI) (11).

2.2 CLINICAL ASSESSMENT

As noted, PE symptoms are often unspecific, and many patients present with a mixture of symptoms as described above. In addition to the symptoms already described, patients with a major PE can suffer syncope, reflecting right ventricular failure or may be hemodynamically unstable. Common characteristics for patients with PE include ≥60 years, a heart rate of 100 beats per minute, 20 respirations per minute and either sex (12). The D-dimer blood test and the clinical scores algorithm are established tools for the clinical diagnosis of PE. D-dimer units are produced from the degradation of crosslinked fibrin (monomers and polymers) units

that are found in blood circulation (13). D-dimer levels are also high when a VTE is present. However, increased levels of D-dimer are also found in patients with inflammatory disease, infections, cancer and post-surgery, and therefore this test has a low specificity to diagnose VTE (14). Different types of D-dimer test are available and so it can be difficult to compare cutoff levels; a level of 0.4ug/mL or less is considered normal. A retrospective study found that negative D-dimer values can help to exclude patients with suspect PE from CTPA examination (13,15). D-dimer assay shows an overall sensitivity and specificity of 84.8% and 68.4% respectively in patients presenting PE. When patients have a low probability of PE, a negative D-dimer test will help to exclude this diagnosis (16). Bounameaux et al., (17) found that a cutoff off 500ug/L allowed elimination of a diagnosis of PE, with a sensitivity and specificity of 98% and 39% respectively.

The Wells and modified Geneva score tests are also proven clinical instruments to help identify patients with risk of PE (18, 19). Along with the 'Rule-Out' criteria system, these tests are a useful indicator for the clinician as to whether to continue the PE investigation. These scoring methods are presented in the Tables 1, 2 and 3 (20).

Tab. 1

Pulmonary Embolism Rule-Out Criteria		
Age > 50	1 point	
SaO_2 on room air < 95%	1 point	
Heart rate > 100 bpm	1 point	
Unilateral leg swelling	1 point	
Recent surgery or trauma ≤ 4 weeks ago	1 point	
Hemoptysis	1 point	
Previous PE or DVT	1 point	
Hormone use	1 point	
Score	*Risk*	
0	< 2% chance of PE	
≥ 1	Cannot rule out that the patient has PE	

Tab. 2

Wells criteria for PE		
Clinical signs of DVT	3 points	
PE is the first diagnosis or equally likely	3 points	
Heart rate > 100 bpm	1.5 points	
Immobilization for at least 3 days or surgery in previous 4 weeks	1.5 points	
Previous diagnosed PE or DVT	1.5 points	
Hemoptysis	1 point	
Malignancy within 6 months	1 point	
Score	*Risk*	*Prevalence*
0-1	Low risk	1.3%
2-6	Moderate risk	16.2%
>6	High risk	37.5%

Tab. 3

Revised Geneva Score of PE		
Age > 65	1 point	
Surgery or lower limb fracture in past 2 month	2 points	
Active malignant condition	2 points	
Unilateral limb pain	3 points	
Previous diagnosed PE or DVT	3 points	
Hemoptysis	2 points	
Pain in limb palpation	4 points	
Heart rate		
< 75 bpm	0 points	
75-94	3 points	
> 95 bpm	5 points	
Score	*Risk*	*Incidence*
0-3	Low risk	Less than 10%
4-10	Moderate risk	10%-60%
> 11	High risk	> 60%

Tables 1,2,3. Taken from Rahaghi et al., (20) Diagnosis of the Deep Venous Thrombosis and Pulmonary Embolism: New imaging tools and modalities. Clin Chest Med 39 (2018) 493–504 0272-5231/18/. 2018 Elsevier Inc.

2.3 IMAGING METHODS

There are a range of imaging methods that can be used for the diagnosis of acute PE, including standard digital pulmonary angiography, selective thorax angiography, CTPA, Ventilation and Perfusion Scintigraphy (V/Q), and MRI, with or without intravenous contrast media (21).

2.3.1 V/Q

In this test, the ventilation (V) and perfusion (Q) of the lungs are investigated using radioisotopes (usually technetium [Tc99m]), which are bound to a carrier such as albumin. This compound is injected into the blood circulation when studying perfusion and is inhaled when examining lung ventilation. The PIOPED I and II studies were large multicenter trials, which showed the capability of V/Q and CTPA to diagnose PE (22). In PIOPED I, patients were classified as high probability, intermediate, low probability and indeterminate; the V/Q showed a high PE prevalence of 87% in the high probability group, and 89% in the very low probability but when investigating patients classified as intermediate and low probability, the prevalence was 58% and 75% respectively (PIOPED I) (22). In an effort to simplify the V/Q results, PIOPED II split the patients in three categories: high probability, normal or very low probability, and non-diagnosis showing a sensitivity of 85% and a specificity of 93% (9). Of important note, if the diagnostic value of Q/V is normal, then PE can be ruled out. The main drawback to the V/Q scan is the high proportion of non-diagnostic cases, which made up 32% outpatients in PIOPED I (23,24).

The use of single photon emission computed tomography (SPECT), with its multiplanar reconstruction possibilities, improves the accuracy of diagnosis further to levels similar to CTPA (20). A previous study found that a correct diagnosis was obtained with CTPA in 94% of cases in comparison to 74% in V/Q. When modification the diagnostic criteria (24), not including the data from non-diagnostic scan, perfusion scintigraphy could achieve a sensitivity of 78% and a specificity of 98% (24).

2.3.2 Computed Tomography Pulmonary Angiography (CTPA)

Remy-Jardin et al. reported two studies from 1992 (25) and 1996 (26) comparing spiral computed tomography (CT) with pulmonary angiography and V/Q, which established the use of CTPA as a reliable tool to depict acute PE. The advantages of CTPA are the speed of examination, the high image resolution obtained, the possibility of all-day examination and the fact that information can be obtained not only from the pulmonary arteries but also from the surrounding parenchyma and heart. The direct visualization of a thrombus is possible due to the presence of intravenous contrast media surrounding the thrombus creating an imageable difference. In the axial plane, when contrast media surrounds a thrombus, it can resemble a “polo mint”; when the vessels and thrombus are detected in the long axis, it may look like a “railway sign”. A thrombus that is found in the central arterial anatomy, between the right and left pulmonary arteries, is known as a saddle thrombus. However, thrombi may also be seen in the peripherical anatomy, in the distal segmental or subsegmental arteries, because of the good image resolution (9).

CTPA has a good sensitivity at 83% and when combined with CT venography it may achieve 90% (21). A follow up study that included 100 patients with a negative CTPA demonstrated no increase in either mortality or morbidity after 6 months (27). The PIOPED II study revealed a specificity of 96% for CTPA to detect PE, however, it did not have great sensitivity (83%). These results were determined from retrospective analysis, as many of the centers involved in the study used just 4 CT scanners. Another study using a Helical CT found a low sensitivity of 70%, making it difficult to rule out PE (28). The high resolution available in a multi-detector CTPA (64, 256 detectors) can visualize distal contrast defects in the peripheral arterial tree (Figure 1), which are present in 1–5% of patients suspected of having acute PE (13).

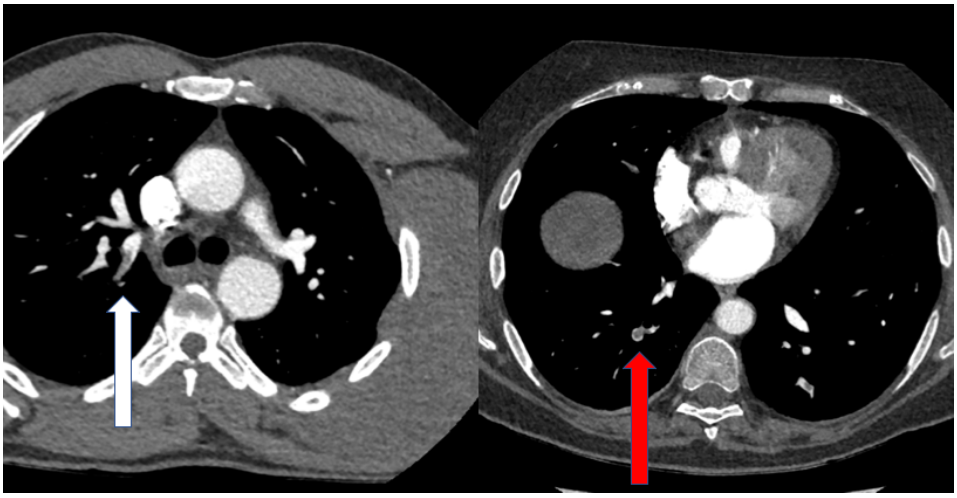

Figure 1: CTPA of two different patients. The LHS image shows (white arrow) a PE in the upper right lobe, at the segment level; the RHS image (red arrow) shows a PE in the lower right lobe in the subsegmental level

Discussions have been held as to which method should be considered the gold standard for PE detection. The pulmonary angiography should be performed in those patients that have a negative CTPA, but present with a high clinical suspicious of PE (29). At present, multidetector CTPA is the diagnostic imaging test of choice for patients with suspected PE. According to the new European guidelines, patients with a negative CTPA, together with presentation of a low or intermediate probability of PE should be sufficient to rule out PE. However, a negative CTPA in patients with high risk of PE should provoke clinicians to make further investigations (30).

Precautions must be taken when using iodine contrast agents in the older population, oncology patients with regard to kidney function, or in the younger population during pregnancy. More than 40% of patients over 60 years old have impaired renal function. Therefore, it is important for this group of patients to have an alternative PE detection technique that is not dependent on the use of intravenous contrast media (31,32,33).

2.4 MAGNETIC RESONANCE IMAGING (MRI)

In recent years, technical improvements in hardware and software, as well as the increased availability of MRI scanners in many centers, is making the use of this imaging method more common. MRI is now commonly used in the diagnosis of neurological disease, in the whole abdomen especially in cancer diagnosis, and more recently, in the thoracic region, when looking after tumor, metastasis or heart and vessels pathologies. There is an unmet need for a diagnostic method for patients with suspect PE and DVT, particularly in those who have a contraindication to intravenous contrast media (34,35). Many authors have investigated different types of approach to avoid the use of contrast media when using MRI to depict PE or have combining the use of Gadolinium contrast media and fast imaging acquisitions, mostly based in the balance steady state free precession (b-SSFP) sequences.

2.4.1 MRI using Gadolinium (Gd) Contrast media

Since 1990, the use of intravenous Gd has been tested for use in MRI angiographies, predominantly in the brain, abdomen and lower extremities (36). PIOPED III, another large multicenter prospective study, demonstrated the possibility of diagnosing PE using contrast enhanced MR angiography (MRA) (Figure 2). The use of intravenous Gd chelate, used to produce a contrast difference between the blood-containing gadolinium in the circulation (high signal) and the pulmonary artery containing a thrombus (low signal), to detect PE was validated. The results showed a specificity of 99%, but a poor sensitivity of 78% in patients with PE. The low sensitivity was related or attributed to the poor technical quality of many of the examinations included the study (11% to 52%). The major issues were poor timing in the detection of the arrival of the injected contrast media bolus, poor or non-breath hold capabilities of the patients, movement, and the sequence itself, with some fold-over artefacts. The study suggested that the use of this technique in centers where the staff were well-trained with the appropriate technical capabilities, should improve the sensitivity of the method (37).

With the improvement of hardware that allowed the use of 3D fast gradient echo techniques, a further study demonstrated the capability of MR angiography to detect PA in comparison to pulmonary angiography. However, the results at the subsegmental level were less than optimal (38). In a large study conducted by Revel et al. (39) using a combination of sequence types with and without Gd contrast media, the sensitivity obtained was as high as 98 to 100%, but these measurements were obtained in the most central part of the lung's arteries. In the segmental and subsegmental areas, the sensitivity dropped to as little as 21% to 33% (39).

Another study by Revel et al. (40) showed that contrast enhanced angiography had a better sensitivity than unenhanced free-breathing sequences for detection of PE. Kalb et al., (41) also discussed the benefits of combining different sequences with and without Gd. They compared the sensitivity of PE detection when using a single sequence such us MR angiography, or a combination of different sequences (MR angiography, 3D GRE and True Fisp), and revealed a change in sensitivity from 55% to 84%.

Nagle et al., (42) described the importance of a dedicated institution where a standardized MRI angiography protocol would be used. They suggested that it should employ knowledgeable staff with the ability to perform highly qualitative MR angiography with Gd contrast media (Figure 2), in order to diagnose the presence of PE.

Figure 2 Showing the use of intravenous injection of Gd to achieve a very good contrast to noise ratio between the vessels and the surrounding tissues. The MRA technique requires the patient to be able to hold their breath during the acquisition, which is not always possible in patients presenting with chest pain or dyspnea.

A morphological approach is not the only method tested to depict PE when using injection of Gd. A dynamic contrast enhance sequence, with acceleration and view sharing technique, can be used to demonstrate perfusion defects in patients presenting acute PE, without the need for breath holding (43,44).

2.4.2 Gadolinium Contrast Media

Gadolinium-based contrast agents have been used over the past three decades and historically the safety of these contrast agents has been shown to be very good (45). The prevalence of severe allergic reactions is exceptionally low (0.001%) and mild reactions are also rare at 0.004 –0.7% (18). However, Gd contrast agents are contraindicated in patients with impaired renal function or during pregnancy. In addition, Thomsen et al., (46) described the occurrence of Nephrogenic System Fibrosis (NSF) when using intravenous Gd contrast media in patients with limited renal function. In the United Stated, a careful approach to the use of Gd-based contrast media has been taken in patients presenting a glomerular filtration rate (GFR) below 30mL/min/1.73m2. Furthermore, the guidelines from the Food and Drug Administration (FDA) and the European Society of Urogenital Radiology (ESUR) are that three of the Gd based contrast media, Gadopentetate (Magnevist®), Gadodiamide (Omniscan®) and Gadoversetamide (OptiMark®) are contraindicated in patients with a GFR under 30mL/min (47). The use of a chelate is essential for the safety of the patients, to guard against toxicity of the gadolinium ion Gd+3, which is a well-documented problem. The chelate isolates the GD+3 from the body tissue and then remains bonded throughout renal excretion. The properties or capacitance of the chelate bond and its stability is related to the chelate structure. Contrast media have a linear or macrocyclic structure and are ionic or nonionic (45). The contrast media named above are all linear in structure and were used in many cases of patients presenting with NSF. The consensus is that those with a macrocyclic structure are safer and more stable; some examples of these are ProHance® from Braco, Gadovist® from Beyer Health Care, Dotarem® from Guerbet, and Clariscan® from Nycomed.

In recent years, it has been found that Gd contrast media can accumulate in the brain and in the bone matrix, leading to further caution when its use. These conditions are termed Gadolinium storage condition and Gadolinium deposition disease (45), (48,49). The International Society of Magnetic Resonance in Medicine (ISMRM) and other institutions suggest caution in using Gd, avoiding its use unless necessary, and that care should be taken if repetitive and control examinations using Gd are needed (49).

2.4.3 MRI without Gadolinium Contrast Media

Due to these health concerns, the medical community working with MRI has an interest in developing sequences, techniques and protocols where contrast use can be reduced or removed. It should also be considered that in some patients, the introduction of an intravenous catheter can be difficult, stressful to the patient and time consuming; the development of techniques that avoid catheterization are welcome.

The use of techniques avoiding intravenous contrast media have been tested and employed for many years when arteries and veins are the imaging target (50). Time of Flight (TOF) is a well-known 2-dimensional (2D) and 3-dimensional (3D) technique, in the brain and peripheral vessels. TOF utilizes the inflow effect of the spin into the slice to be acquired; its limitation is the length of time taken acquiring the slices, while the anatomy of the vessels should be perpendicular to the slices for the best results. The Phase Contrast (PC) technique is also well know, and often used in the brain with an excellent background suppression or for measuring arterial flow (51).

Non-contrast Magnetic Resonance Angiography (MRA) using ECG-synchronized 3D Fast Spin Echo (52) is a useful technique for imaging the lower legs and chest which does not use contrast media. The technique is based on a difference in signal and contrast between blood flow during systole and diastole. During systole, the arteries present a signal void because of the high flow while the veins give a high signal; during diastole, the veins and arteries both present a high signal. Subtraction of both images produces the arterial signal alone (see Figure 3). A disadvantage to this technique is a long scan time and the risk of patient movement between the two different images, causing motion artefacts and a poor subtraction image as a result. ECG is needed to quantify the time delay of the arterial inflow to the region of interest, which is not always an easy procedure.

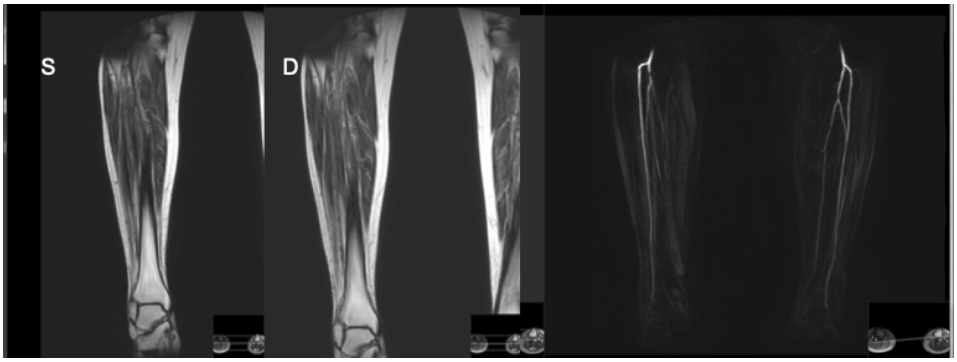

Figure 3 An example of the non-contrast MRA, TRANCE technique Fast Spin Echo, using electrocardiogram synchronization of the images in systole (S) and diastole (D) phases to produce the final subtracted image to the right.

In contrast to the previous technique, Arterial Spin Labeling (ASL) employs the inflow or outflow of blood into a region which is pre-saturated with an inversion recovery pulse. Thus, stationary tissue is suppressed, and so generates a particularly good contrast to noise ratio in the image to aid the visualization of the blood vessels, with background suppression as a

result. This technique can be used with half-Fourier Fast Spin Echo (FSE) or with a balanced Steady State Free Precession (b-SSFP), both of which give a high signal from the blood. The fast spin echo technique is dependent on the flow and the direction of flow, while b-SSFP is independent of the flow but suffers from magnetic field inhomogeneities. A general 'recipe' when using this technique is to use FSE when medium to slow blood flow is targeted, while b-SSFP should be used when the blood flow is fast. Okuaki et al. (53) demonstrated the capability of this technique with inversion saturation pulses to separate the veins from the arteries in the lungs. Many further studies have tested different approaches in ASL, using two or three different pre-saturation or inversion pulses to obtain a completed saturated background with blood flow given a high signal intensity due to the labeled protons (54,55).

2.4.4 Balanced Steady State Free Precession

In recent years, there has been an increasing interest in developing fast methods for chest MRA, which require less effort and compliance (allows normal breathing) from patients, and abolishes the use of intravenous contrast media, both of which improve the patient experience.

The b-SSFP sequence is a popular technique for fast imaging and provides good contrast between tissues and vascular territories without the need of intravenous contrast media. TrueFISP (Siemens Healthcare), Balanced FFE (Philips Healthcare) and FIESTA (GE, Healthcare) are the most common names used by vendors for this kind of sequence, which belongs to the family of Gradient Recalled Echo (GRE). In contrast to a standard fast spin echo sequences, where a choice of T1 or T2 contrast is made to obtain a desired contrast weighting in the image, the b-SSFP contrast weighting depends on the ratio between T2/T1. Fluid and fat tissues have a large difference between T1 and T2 relaxation times that result in a bright signal, but as the ratio is similar, the signal intensity coming from fat and fluid in a b-SSFP will be similar (56,57).

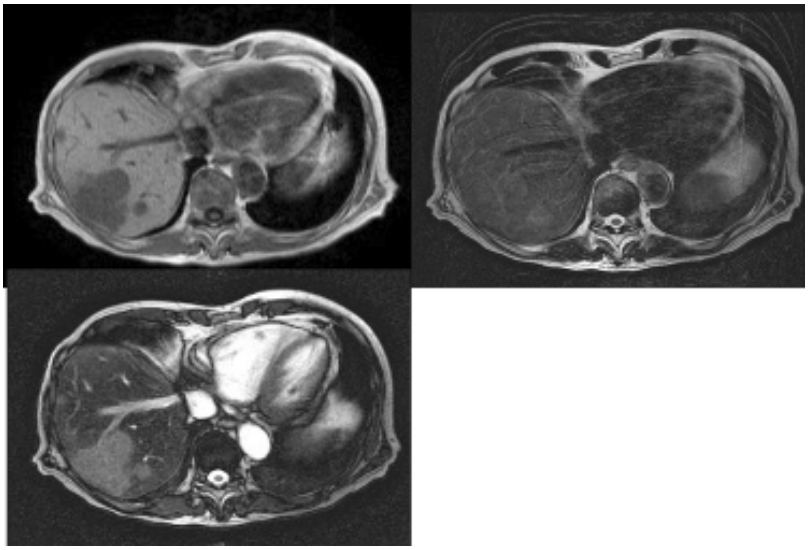

Figure 4 The upper left panel shows a T1w image providing a high signal from the fat and liver, and low signal from the heart, vessels and fluid. The upper right panel shows a T2 w image with a high signal from fluid and fat, and a low signal from vessels and heart. The bottom left panel shows b-SSFP, presenting a contrast mixture of T1 and T2 weighted image, with a high signal in the vessels/blood, heart and fluid.

This fast image technique has the advantage of a high signal-to-noise-ratio (SNR), and a very good contrast-to-noise-ratio (CNR) (Figure 4). In this sequence the blood presents with a high signal (Figure 5a and 5b) and the patient received a low deposition of energy compared to spin-echo techniques. (58). Non-balanced GRE sequences, such as Fast Low-Angle Shot (FLASH) often utilize a short TR and disrupt or spoil the transverse magnetization at the end of the repetition time, resulting in a T1-weighted image in what is often called spoiled GRE. In a balanced GRE, the transverse magnetization from the previous excitation is refocused and will contribute to subsequent repetitions. This results in a mixture of a T1 and T2 weighted image contrast. To achieve this, a very short repetition time is needed, which is briefer than the T2 and T1 relaxation time of the tissues, and an echo time which is exactly half the repetition time. The mixture of contrast weightings and the high signal obtained in the images is made possible because in addition to the GRE, the free induction decay and the residual transverse signal are both used to produce the measured signal. Because of the high SNR, higher resolution images may also be acquired.

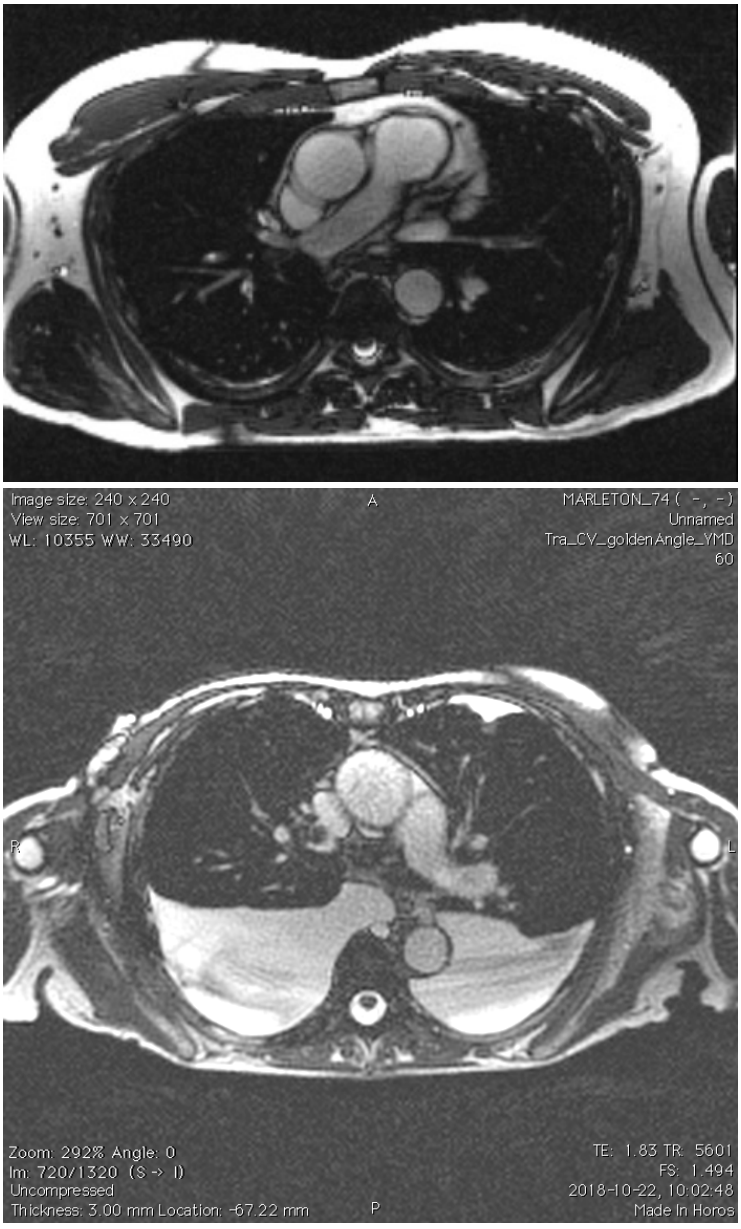

Figure 5 a) the upper panel shows an image example of a balanced steady state free precession, which shows high signal intensity from the main lung's arteries, aorta and fat and the bottom panel 5b) shows also a balanced-SSFP with high signal intensity from vessel and pleura fluid (Vargas Paris et al.)

Heye et. al. 2014 (59) demonstrated the capability of ultra-fast SSFP when looking at the pulmonary anatomy in a single breath hold. In the IRM-EP study (39) 274 patients were

included. It used both a Gd-enhanced MRI angiography technique, and a non-contrast imaging approach when combining with SSFP sequences to find an overall sensitivity to detect pulmonary embolism (PE) of 68.9 to 75%; the highest sensitivity was in the central anatomy of the lung's arteries, achieving 97.7 to 100% (40).

Other authors have chosen to compare the capability of b-SSFP to standard 3D GRE T1w post Gd and found a good visualization of arterial anatomy in pregnant patients (60). The use of b-SSFP also allows the possibility to examine not only PE but also to investigate whether patients have a deep vein thrombosis (DVT) (61).

A common approach is to scan each slice a number of times, producing several images per position to examine the lung's arteries (62,63,64). The Nyren at al., study repeated every single slice position five times in three different planes, using a b-SSFP based sequence (Figure 6). They obtained a sensitivity of 90 to 93% with a 100% specificity. Another study (32) tested the ability of b-SSFP to depict both the central and peripheral vessels in the lung. They used a radial sampling technique called quiescent interval slice selective (QISS), also a non-contrast medium based sequence, to depict the anatomy of the lung's arteries in volunteers. They suggested that further studies should be performed in patients with suspected PE to prove the accuracy of this method.

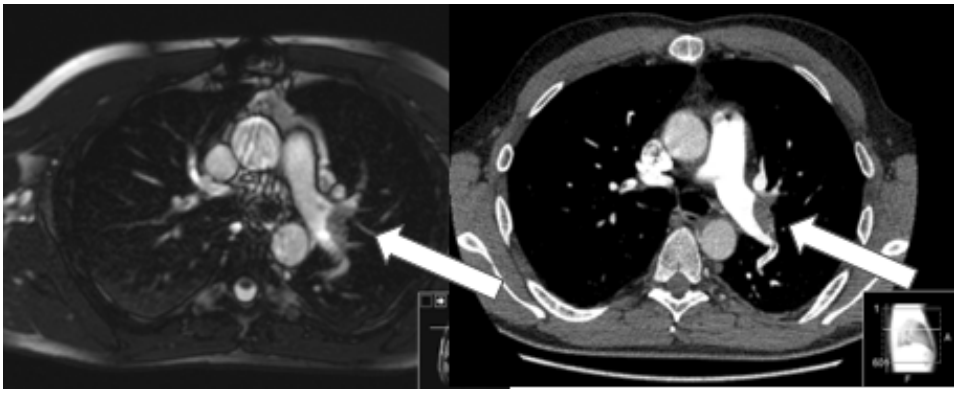

Figure 6 The left panel shows a b-SSFP image, right panel shows a CTPA image; white arrows depict PE in the main left lung artery (Nyrén et al.) (62).

2.4.5 Diffusion Weighted Imaging (DWI)

Diffusion weighted images provide information from the random, spontaneous movement of water in a tissue, which is Brownian motion. In most organs in the body, the number of cells

and membranes determine if water has normal or restricted random movement. Therefore, DWI will show the degree of diffusion, and in some cases the indirect degree of cellularity of a certain tissue or how much space the tissue has, between cells in the inter or intracellular space. The intravascular water movement will also be reflected in the amount of signal depicted from the DWI. In the brain, water can move over a distance of 10μm in a period of 50 msec while the sequence is depicting the signal (65).

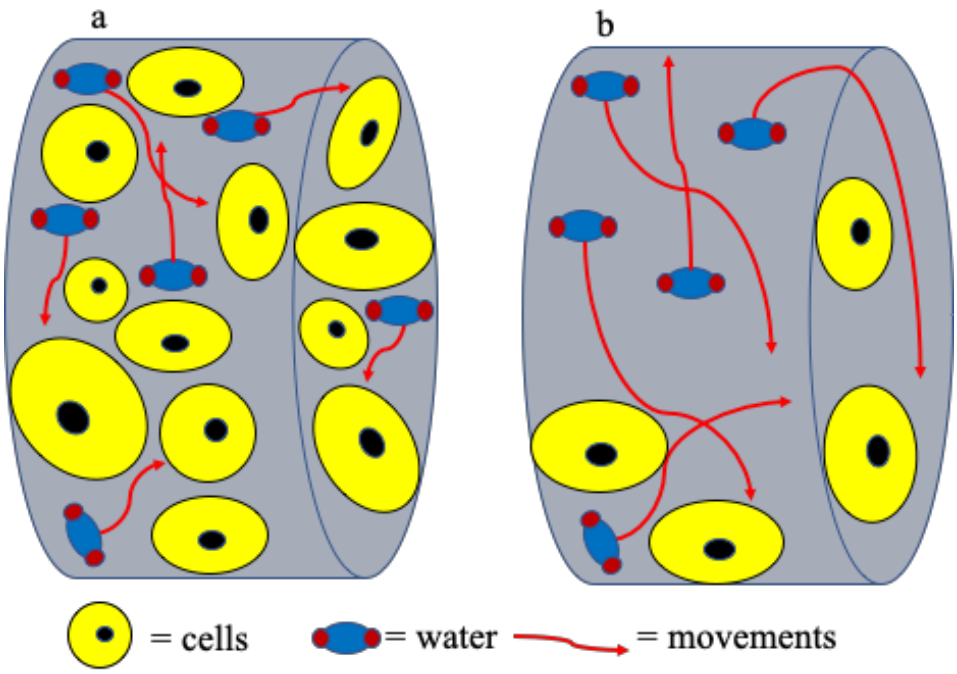

Figure 7 Cells (yellow circles) and water protons (little blue and red dots) in two tissues with different cellularity showing variable diffusivity, a) restricted diffusivity; b), non-restrictive diffusivity.

DWI is a powerful tool, not only for diagnosing neurological diseases like stroke, but also in oncology, allowing measurement of water diffusivity into different tissues (Figure 7) of the body (66). A fast Echo Planar Image (EPI) technique together with new shimming algorithm has made it possible to perform DWI in abdominal imaging of the kidneys and liver, for detection and characterization of different lesions (67). Major improvements in hardware, for example faster gradients and better receiving coils along with relatively new software such as parallel imaging, sensitivity encoding (SENSE) (68) or generalized auto calibrating partial parallel acquisition (GRAPPA), have allowed examination of the thoracic region and lungs with fewer artefacts. (66, 69, 70).

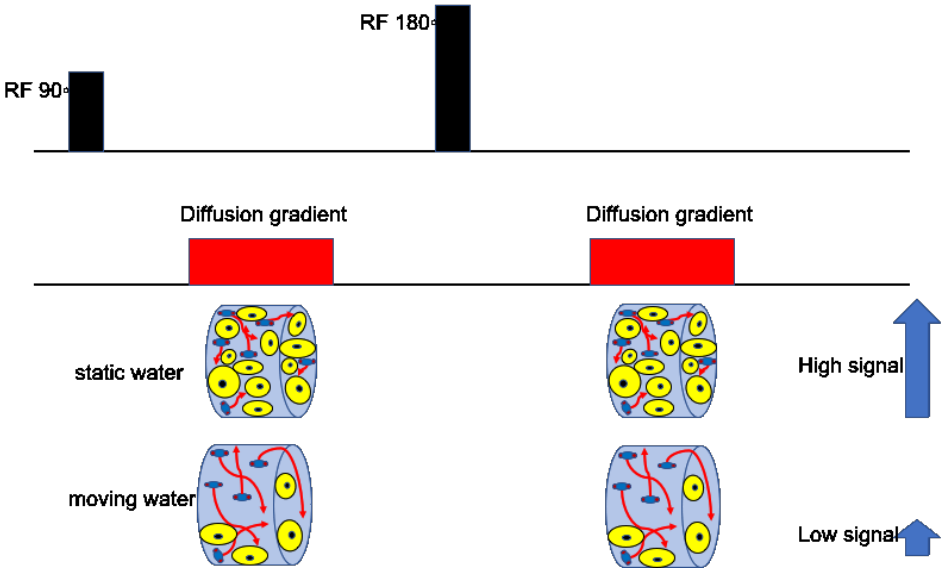

Figure 8a Diagram of DWI pulse sequence showing the difference in signal intensity when the water molecules are static resulting in a high signal or when they are free to move, presenting low signal intensity.

Adapted drawing from Stejskal and Tanner DWI sequence diagram. (1965). Spin Diffusion Measurements: Spin Echos in the Presence of a Time-Dependent Field Gradient. The Journal of Chemical Physics 42:1, 288-292

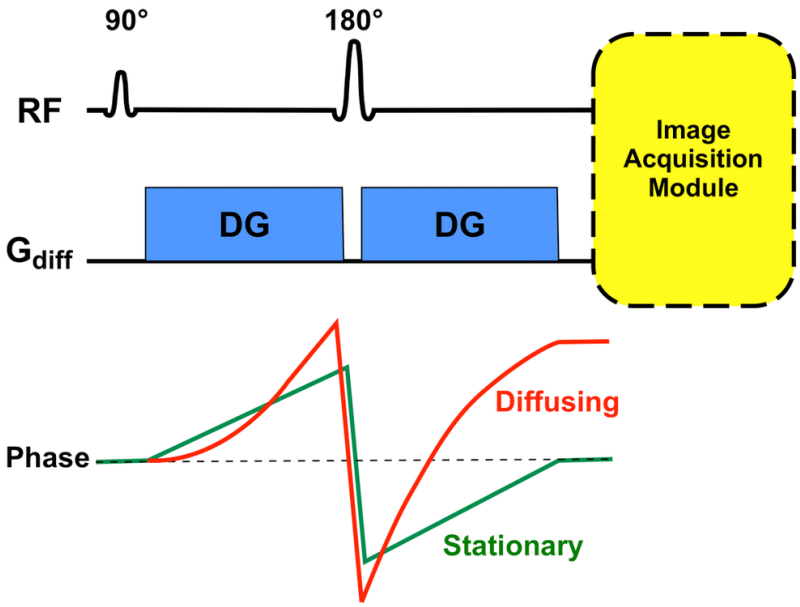

Figure 8b. Showing the high signal obtaining from stationary water molecules and the lack of signal from diffusing water molecules. Courtesy of Allen D. Elster, MRIquestion.com. Copyright© 2020 AD Elster, ELSTER LLC.

Stejskal and Tanner (71) have described a sequence (Figure 8a) that allows visualization of the signal differences between static molecules (high signal) and those with sufficient room to move (low signal). The static water molecule phase will be lost when the first diffusion gradient is applied but will be rephased following application of the second diffusion gradient, resulting in a strong signal (Figure 8b). Conversely, when water molecules move, they will experience different gradient strengths. The water molecule will be in position 1 when the first gradient is applied, but as it moves to position 2 during the second gradient application, it will not be able to completely rephase those protons, and consequently the result will be the loss of signal.

The level of sensitivity of this diffusion measurement will depend on how long and strong together with the spacing between the application of diffusions gradients. In clinical practice, the parameter that determines how sensitive is the sequence is to measure or depict diffusivity or proton movements is called the b value. A low b value will be sensitive to detect large movement of water molecules, for example as in urine in the bladder or intravascular water. A b value of around 50 or 100 s/mm^2 is classified as low or short. A b value of 1000 s/mm^2 is required to detect a small water molecule movement. The sequence will be sensitive enough to detect tiny movement of water molecules traveling small distances, presenting the normal diffusivity without signal (70).

2.4.6 Restrictions when using DWI

The echo planar imaging technique is a rapid way to collect diffusion data in the k-space, but it is susceptible to artefacts when the field of view is inhomogeneous and a chemical shift in the region of interests is present, producing degradation of the image quality (72). Other problems can occur, such as misinterpretation of high signal intensity because of a long T2 relaxation time in some normal tissues (so-called shine through) which is not due to restricted diffusion.

When at least two b values are measured, it is possible to obtain a quantification of the degree of diffusion, a how much the water moves. This in known as an Apparent Diffusion Coefficient (ADC). A line may be plotted between the signal intensity of the tissue at the different b values and the slope obtained provides the ADC value. This implicates that the more b values available, the greater the accuracy of the ADC obtained but with a longer acquisition time.

A well-known problem with DWI is the presence of an inhomogeneous field, when different tissues interface close to or adjacent one another, for example like air or bone near a soft tissue, inducing susceptibility artefacts and distortion to the images (65, 67). Nevertheless, the improvement of DWI imaging, using a multi shot technique for example, has allowed the detection of tumors, tissue characterization, or follow-up tumor treatment in the body (70). In our institution, DWI imaging is involved in almost all tumor or cancer imaging protocols, including those for prostate, breast, liver and rectal cancers. Because of the modernization and recent technical improvements, is also possible to use DWI in the evaluation of the whole body, detecting metastasis and staging cancer patients (73,74). Meier-Shroers et al. (75), studied the use of MRI for lung cancer screening in high risk patients, showing an exceptionally good sensitivity and specificity, detecting lymph nodes around 6 mm in size. Another study attempted to evaluate the malignancy or benignancy of thrombosis in the liver, in patients with hepatocellular cancer using DWI (76). Catalano et al. (77) also investigated the effectiveness of DWI to differentiate benign from malignant thrombosis in patients with hepatocellular carcinoma, while Ahn et. al. (78) used DWI to differentiate benign portal vein thrombosis from malignant type, and in this case with no positive results. Overall, DWI can be used to depict thrombosis (Figure 9).

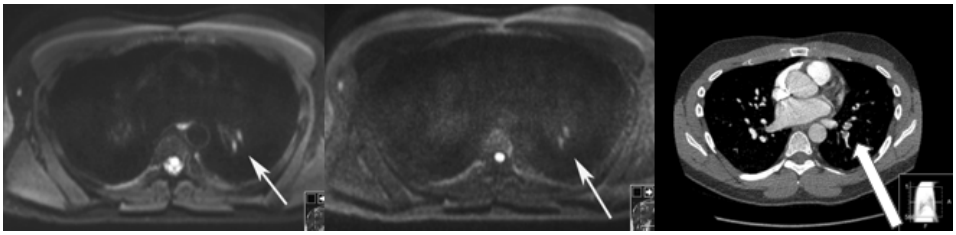

Figure 9. Shows in left and middle, DWI at b=50 and b=800 and right image a corresponding CTPA, two PE in the left lower lobe (white arrows) (Vargas Paris et al.)

2.5 COLLECTING THE MR SIGNAL

2.5.1 Cartesian and radial approaches

There are varying approaches for MRI raw data collection. The most common is Cartesian grid sampling, while data may also be collected in a radial (figure 10 a) or and spiral fashion which are colloquially know as non-Cartesian methods. Recent studies have suggested that data may also be collected randomly. Efforts have also been made to speed up raw data sampling by under sampling the k-space and using a reconstruction technique called compressed sensing to obtain good quality images (79). Cartesian sampling data is collected in parallels lines through the whole k-space. In most of the sequences, the data lines are collected after every TR and this makes the process directly dependent on the number of repetition times and the time between each repetition. A moving patient or organ will produce a phase disparity between lines, resulting in ghosting artefacts in the image. This often occurs due to respiration when imaging the thorax or due to peristalsis in the abdomen. If data points are collected at different times and from different positions of an organ due to movement, this will degrade the image quality (80).

There are strategies available to overcome the artefacts produced by movement. External devices can help to synchronize the data collection during respiration and overcome artefacts; these can include a respiratory belt or the use of an electrocardiogram (ECG) to monitor the heartbeat. This will also increase the acquisition time and reduce the overall efficiency of the examination time (81). Another approach is to ask the patient to breath hold, but this limits the attainable resolution and scan times of the images and is not suitable for all patients. Another method is to use a non-Cartesian method called Periodically Rotated Oversampling Parallel lines with enhanced reconstruction (PROPELLER) where a data block containing a number of parallel lines is acquired. After every repetition time, the block is rotated to cover a different part of the k-space (Figure10b). After several rotations, the data obtained will nearly

cover the whole k-space. This results in oversampling data at the center of the k-space, and so reduces the artefacts (82). Vendor-specific names for this method are BLADE (Siemens Healthcare) and MultiVane (Philips Healthcare) (75). The main benefit of this radial technique is the reduction of artefacts from movement (75,83).

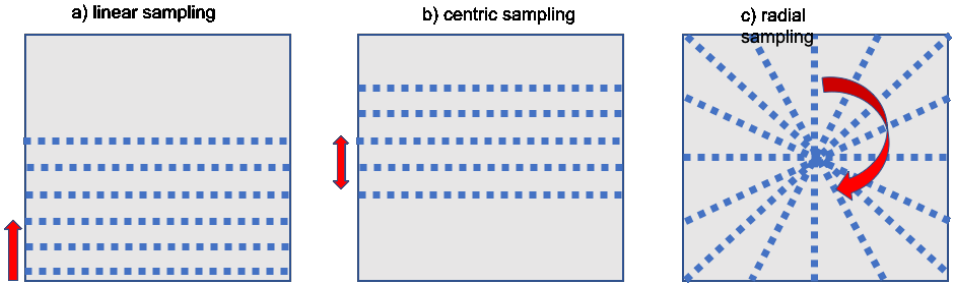

Figure 10a. Cartesian sampling with linear (a), centric (b) phase encoding in comparison to radial sampling (c) of the k-space. In this example, the width of the data block is a single line. Adapted from Fyrdahl et. al. (2018). Copyright © 2018 International Society for Magnetic Resonance in Medicine. Published by John Wiley & Sons Inc.

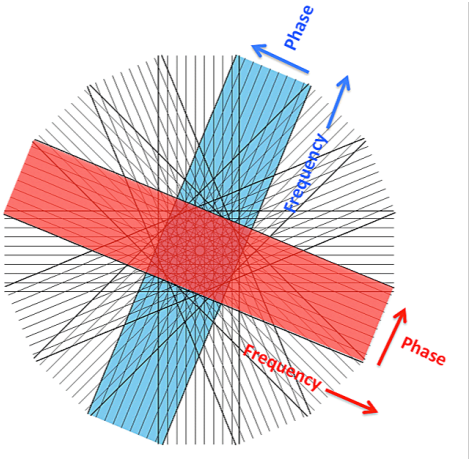

Figure 10 b. Shows a PROPELLER sampling approach. Courtesy of Allen D. Elster, MRIquestion.com. Copyright© 2020 AD Elster, ELSTER LLC.

A relatively new method to reduced artefact involves the collection of raw data in a random fashion, which is then reconstructed using a compressed sensing technique; this may, in the future, provide a good image quality, with fewer motions artefacts, short scan times and flexibility of post reconstruction images, with different temporal resolution (84).

2.5.2 Golden angle in radial sampling

Another approach to sampling is to collect a single line of data for each repetition time and then rotate a certain amount of degrees when collecting the next line (figure 11). This radial acquisition technique has several advantages. One is that motion artefacts appear as streaking lines over the image, with much lower intensity than Cartesian images. The artefacts will be spread in the whole image, with less signal intensity, because the lines pass through the center of the k-space every repetition time (85). Azevedo et al. (86) used a radial GRE in patients, in both adults and pediatric patients with breath holding difficulties and found that the use of a 3D T1 weighted GRE radial sampling was feasible when scanning the abdomen.

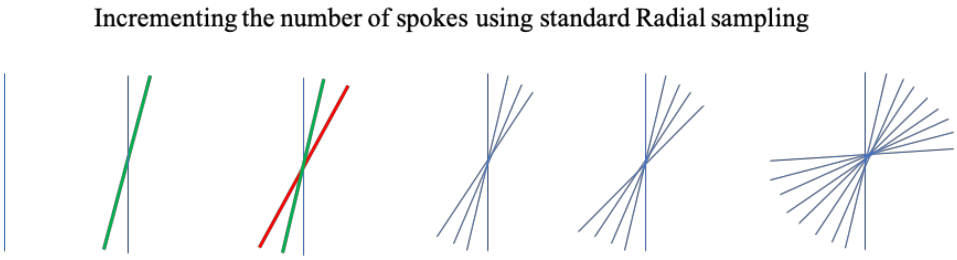

Figure 11 Simulation of the standard radial sampling distribution of lines collected in k-space in a certain period of time.

Another popular radial method is the golden angle approach, which uses an incremental technique determined by dividing 180 degrees by the golden ratio. The most common approach is to use the larger of the two resultant angles (111.246 degrees). This increment keeps the distribution of the lines ‘well dispersed’ over the k-space, independent of how many lines are collected (Figure12). The gap between two adjacent spokes can only be one of three different angles. If the number of lines is a Fibonacci number, then only two different gaps occur. The distribution of the lines, independent of number collected, allows for a huge flexibility in the reconstruction. The reconstruction can be made using many lines after a certain time to obtain a good resolution and SNR but with poor temporal resolution. The reconstruction may also be made from fewer lines from the same collection, obtaining several images with high temporal resolution (Figure 13). This post-reconstruction technique is called the ‘sliding window’ (87).

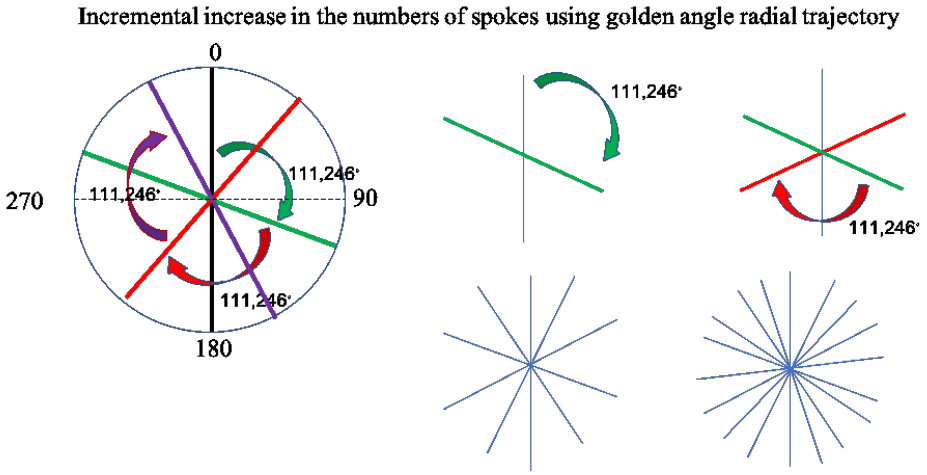

Figure 12 Example of golden angle radial sampling achieving more symmetrical distributions of the lines over the k-space, over a certain period of time.

In recent years, a number of publications have detailed the use of radial sampling with the golden angle approach and post-reconstruction capability (88, 89). Stroud et al. (90) used this technique to examine the whole heart and the thoracic aorta to improve image quality when using golden angle sampling. Other investigators have used the possibility of extracting respiratory movement information from golden angle sampling to improve image quality, without the need for an external device to capture the movements or a breath hold technique (91, 92). In abdominal and thoracic imaging, the movements of chest and abdominal wall reduce the quality of the images.

When using the golden angle approach, a post reconstruction technique, can be used to improve the image quality, resulting in fewer motion artefacts (93). This reconstruction technique also allows the possibility to obtain images with high temporal resolution, (94, 95) or to allow post-reconstruction of the radial samples obtaining different slice thickness and position when scanning with continuous table movements (96).

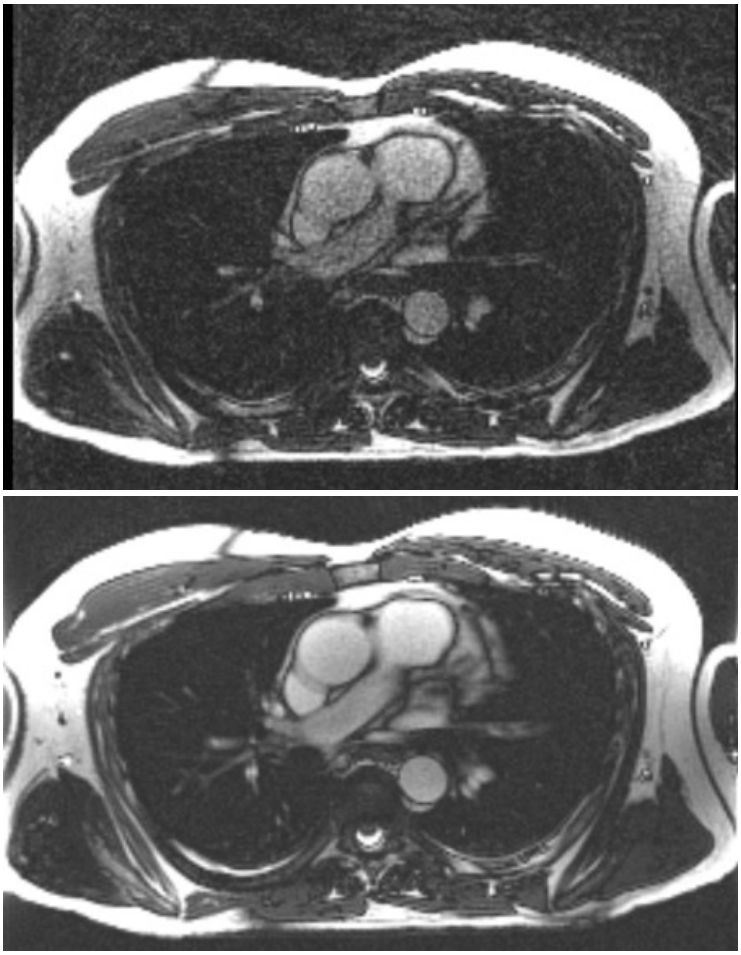

Figure 13. The upper panel shows a golden angle radial image reconstruction using 144 spokes and the bottom panel shows a reconstructed image using 1345 spokes.

Vargas Paris et al.

3 RESEARCH AIMS

3.1 THE AIM OF THE THESIS

The overall aim of this thesis was to investigate the capability of different magnetic resonance sequences to depict acute pulmonary embolism (PE).

3.1.1 Study I

The aim of this study was to demonstrate the capability of balanced steady state free precession (b-SSFP), using a repeating slices position approach and in three different orthogonal planes, in patients with acute PE.

3.1.2 Study II

The aim of this study was to demonstrate the capability of diffusion weighted imaging (DWI) depicting acute PE

3.1.3 Study III

The aim of this study was to test a new radial sampling technique to improve image quality in b-SSFP when imaging the pulmonary arteries.

3.1.4 Study IV

The aim of this study was to test the clinical capability of the radial sampling approach (Study III) a golden angle radial b-SSFP when examining patients with suspect acute PE

3.1.5 Study V

The aim of this retrospective study was to analyse all patients who only examined with MRI only if their physician suspected the presence of a PE, and thereby assess the potential of MRI alone to diagnose acute PE.

4 MATERIALS AND METHODS

4.1 STUDY I

4.1.1 Patients and volunteers

We scanned 33 in-house patients with suspected PE consecutively. All MRI examinations were performed after computed tomography angiography (CTA). This cohort consisted of 10 women and 23 men with an average age of 48 years. As most of the patients were true positive, a group of 37 volunteers (22 women) were also included in the patient's sample.

4.1.2 Imaging protocol

The CTA was performed on a Lightspeed VCT scanner (GE, Healthcare, Milwaukee, WI, USA). All patients and volunteers were also scanned with a 1.5 T MRI scanner (AERA, Siemens Healthcare, Erlangen, Germany), with a Torso coil and 18 different coils elements. A 2D b-SSFP sequence was used, with a TR/TE of 2.8/1.23 ms, 4.5 mm slice thickness with a negative gap of 60%. Pixel resolution was 0.9 x 0.9 mm. The flip angle was 70^0. Three different orthogonal planes were scanned (transversal, sagittal and coronal) and every slice position was repeated 5 times. Neither triggering or breath holding techniques were used when scanning with b-SSFP.

4.1.3 Image analysis

All data and MRI images were blinded for analysis by two radiologists (R1, R2). A specialist thoracic radiologist reviewed the CTA and was not given any information collected from the MRI examinations. In cases where there was no consensus of results (MRI vs. CTA), a further review was made. Different pulmonary territories were evaluated, for example, the central arteries, lobes, segment and subsegment arteries, in the right and left side of the body. We calculate the sensitivity, specificity, the positive, and the negative predicted values.

4.2 STUDY II

4.2.1 Patients and volunteers

We recruited 20 in-house patients who had PE that had been verified with CTA. Sixteen men and 4 women were included, with a mean age of 59 and 57 years respectively. Mean waiting time between the CTA and MRI was 26 h. Because the cohort did not include any PE-negative patients, a group of 20 healthy volunteers were also recruited, consisting of 16 women, and four men of mean age 45 and 43 years respectively.

4.2.2 Imaging protocol

All patients and volunteers were scanned with an MRI 1.5T (AERA, Siemens Healthcare, Erlangen, Germany). A torso coil with 18 coils elements combined with a spine coil were used. The initial scan made was a transversal b-SSFP with TR/TE 3.6/1.3 ms, 0.9 x 0.9 x 4.4 mm^3, slices 90, which was used as an anatomical reference. The second scan was a single shot echo planar diffusion weighted imaging at the same plan. Three different b values of 50, 400 and 800 s/mm^2 were used with a TR/TE 5600/60 ms and a resolution of 2 x 2 x 5 mm^3. Neither respiratory nor cardiac triggering was used. Patients and volunteers were instructed to breathe normally. IPat factor 2 was used in both sequences.

4.2.3 Image analysis

Open Source Analysis (OSA)

All images were presented as an open source, i.e. the patient's images, CTA and MRI (b-SSFP, DWI), were evaluated at the same time. All images were read using the Picture Archive System (PACS). We used the b-SSFP to guide and confirm the position of a find, due to the poor quality of the anatomical information provided by DWI. A high signal in DWI were confirmed as a true positive if the signal was classified as, in an artery position, when looking the b-SSFP. If no artery correlation was found, then the signal was classified as a lymph node. When a find had high signal for the three b values, we calculated an apparent diffusion coefficient (ADC).

Blinded Diffusion Analysis (BDA)

One year following the initial observation, further analysis was made by two radiologists (Observer 1 and 2); these observers were not given any patient information or CTA images; only DWI images were available to check for any signs of PE (high signal intensity). The results were later correlated to CTA and also to the b-SSFP.

4.3 STUDY III

4.3.1 Patients and volunteers

Ten healthy volunteers (46±11 years) were recruited to the experiment, plus two patients with confirmed PE (CTA validated).

4.3.2 Imaging protocol

The volunteers and two patients were scanned with an MRI 1.5 T (AERA, Siemens Healthcare, Erlangen, Germany) using a Torso coil with 18 different elements and combined with an integrated spine coil. Two different b-SSFP sampling techniques were used, Cartesian (a) and golden angle radial (b) samplings schema (Figure 14), using a sliding window reconstruction technique.

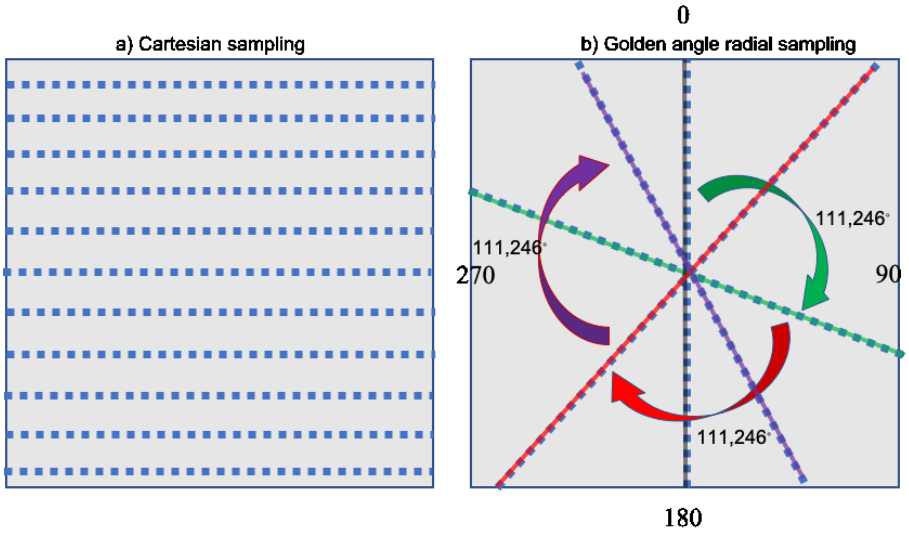

Figure 14 Shows Cartesian a) and golden angle radial b) sampling trajectories.

Cartesian images were made with a TE/TR of 1.8/3.2 ms, with 163 lines covering the raw matrix data, and a temporal resolution of 522 ms. The radial sampling was made with TE/TR 1.8/3.6 ms, a total of 1345 spokes were used to sample the whole raw data space. A retrospective reconstruction was made with 144, 610 and 1345 spokes. Both sequences hade IPat factor 2, and 3 mm slices thickness and covered the same anatomy.

4.3.3 Image analysis

Two radiologists, both blinded to Cartesian and radial sampling, were asked to score the images using a 1 to 5-point scale, where 1 was the worst and 5 was the best image quality possible. The images from the two patients were used to confirm the contrast-to-noise ratio between the blood and the emboli and confirmed by CTA. Three series with different amounts of spokes were generated from the radial sampling. The first was to achieve a reconstruction as close to Cartesian sampling time (144 spokes). The second was a reconstruction with fully sampled data (610 spokes), while the third used all the data

acquired, and all spokes present during the acquisition (1345 spokes). A sharp analysis of the pulmonary arteries was also made in the Cartesian and radial b-SSFP sequences.

4.4 STUDY IV

4.4.1 Patients

We recruited 76 different patients that were referred for a CTA due to a suspicious, acute PE. Sixty-four patients took part in the study. Thirty-three females with a mean age of 68.8, (36-90 years) and 31 males, mean age 62 (27-89). All patients were required to have an MRI examination prior to the CTA. The mean time between MRI and CTA was less than an hour.

4.4.2 Imaging protocol

All patients were examined in an MRI scanner 1.5T (AERA, Siemens Healthcare, Erlangen, Germany) and in a CT scanner, Lightspeed VCT (GE, Healthcare, Milwaukee, WI, USA).

The MRI b-SSFP sequences were the same as those used in Study III, golden angle radial sampling with a sliding window reconstruction, and a Cartesian sample (as per Nyrén et al but with different slice thickness; TR/TE 3.2/1.6 ms, GRAPPA 2, 163 k-space lines) and a golden angle radial trajectory (according to Fyrdahl et al; TR/TE 3.6/1.8 ms with 1345 spokes). Similar parameters for both sequences were flip angle 60^0, receiver bandwidth 1008 Hz/px, FOV 450 x 450 mm^2, and voxel size 1.6 x 1.6 x 3 mm^3. The Cartesian sampling time was 522 ms and the radial sampling with 144 spokes resulted with a time of 518 ms. This was chosen to achieve a similar time between the sequences.

4.4.3 Image analysis

Two different observers (R1 and R2), who were blinded to the CTA images and results, were asked to score the radial sampling for the presence or absence of PE; the scale ranged from 1–2 for negative or normal and probably normal, or 4–5 when they were sure or very sure they had observed a PE, while 3 was used to give bad quality images an score, meaning that if the observer could not give an answer, and the examination should be repeated. We generated a table with 48 different arteries position to be scored, which was divided into central, lobes, segmental and subsegmental, at the right and left lung; this generated 3072 points to be scored.

Six months later R1 was asked to score the Cartesian sampling, using the same scoring system. A third observer (R3) was asked to score blinded images of 64 patient CTAs, using the same protocol as above. R3 also performed an extra analysis of four different patients,

looking only to radial images with three different reconstructions. The time between the observation of the CTA and the MRI image was 3 to 4 months. The reconstructions used 144, 610 and 1,345 spokes generating 12 different observations. The sensitivity and specificity of the golden angle radial and the Cartesian sampling was calculated, and the level of improvement, if any, of PE detection when using different amount of spokes in four patients selected from the group of 64 was investigated.

4.5 STUDY V

4.5.1 Patients

Several patients (2012-2018; 27 women/30 men) could not undergo the standard CTA due to contraindications including renal failure, iodine allergies, pregnancy and radioactive iodine therapy, and so underwent the MRI examination protocol used in Study I.

Information on the quality of the MRI images, the presence or absence of PE, and other findings present in the images, along with the clinical outcome of every patient after three months and one year were extracted from the Electronic Medical Record system (EMR).

4.5.2 Image protocol

All patients were examined in a 1.5 T scanner (AERA, Siemens Healthcare, Erlangen, Germany). A torso coil was used in combination with a spine coil, using the same 2D b-SSFP sequence as in study I. MRI is currently not a standard examination when looking after PE.

4.5.3 Analysis

The standard radiology reporting protocol utilized by the hospital includes two reviewers, the first making a preliminary report, followed by the second who defines the final report; this method was adopted in this study. Several patients, including those who were thought to have PE, received anticoagulation treatment before their MRI. Those patients who had a negative MRI and then presented with a thromboembolism within a year of the EMR reading, were considered as a false negative. True negatives were classed as those who had a negative MRI and no thromboembolism within a year according to EMR. Patients who presented with signs of PE, for example a defect of filling in vessels upon MRI, were considered to be positive for PE. We could not assign false positive results, because of the lack of a reference method.

5 RESULTS

5.1 STUDY I

Results

Of 33 patients in the study, 29 were identified as true positive for CTA. For b-SSFP, R1 detected 27 CTA correctly, representing a sensitivity of 93%. R2 identified 26 cases of CTA correctly, giving a sensitivity of 90%. Both observers showed 100% specificity. Two of the patients with CTA that were not identified by b-SSFP had subsegmental emboli only.

5.2 STUDY II

Results

In terms of OSA, 370 (100%), emboli were identified in the patient group with CTA. The b-SSFP technique found 237 (64%) of those. With DWI, the b value 50 identified 327 (88%), the b value 400 identified 245 (66%), and b 800 identified 138 (37%).

Of the b 50 identifications, 22 were false positive in the patient group and 66 were false positive in the healthy volunteer group. The results of the BDA analysis found a total of 204 emboli; 34 of these were lymph nodes, while 160 were true positives. Later analysis found that 68 of these positive findings could not be correlated to the b-SSFP, while 10 finding were not related to vessels.

5.3 STUDY III

Results

Study III was designed to test a new radial sampling technique to improve image quality in b-SSFP when imaging the pulmonary arteries. Both sequences showed artefacts derived from respiratory motion and flow. The Cartesian technique was most sensitive to these perturbations. The diagnostic quality improved when the number of spokes was increased. The respective scores were Cartesian 2.2 ±0.6, Golden angle 144 spokes 2.3 ±0.7, 610 spokes 2.8 ±0.8 and 1345 spoke 3.5 ±0.9. In one of the volunteers, it was found that ECG triggering improved the image quality the most in comparison to respiratory triggering and breath holding.

Most of the Cartesian images identified severe artefacts especially in the central arteries, when compared to radial sampling, which was associated with under-sampling or streaking artefacts (Figure 15). The scores showed no difference between the sequences. This test demonstrated that radial sampling had the best diagnostic quality and sharpness of image for the vessels.

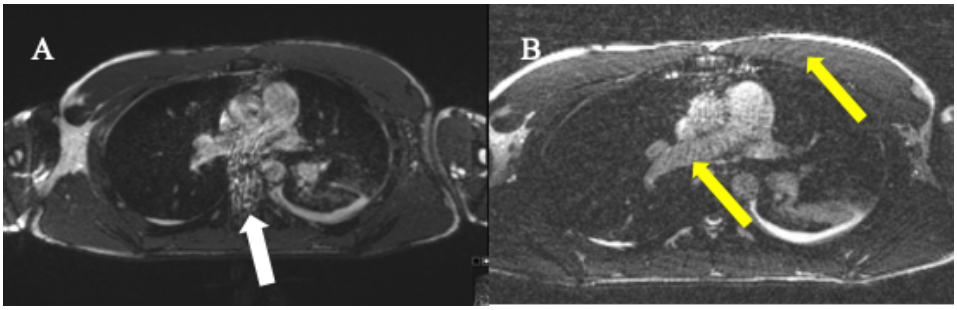

Figure 15 A) Cartesian imaging with flow artefacts (white arrow); B) radial imaging showing streaking artefacts (yellow arrows).

5.4 STUDY IV

Results

From the 64 patients included in this study, a total of 3072 different arteries were observed. CTA identified a total of 183 emboli from this cohort, with R 1 matching 40 of these while R 2 found 32. The best radial MRI results for both observers were found in the right lower lobe region; R 1 identified 23 emboli and R 2 24, with CTPA identifying 66 in total. The least accurate radial sampling results came from the right and left upper lobes; here, in the right-side CTPA identified 27 emboli, while R 1 found 2 and R2 zero. For the left-side, the findings were 18, 1 and zero for CTA, R 1 and R 2 respectively. When comparing the quality of the Cartesian and radial techniques, the results showed poor quality images in 29.7% and 23.4% of the Cartesian images at lobar right and left level. The radial technique revealed that only 2% of the images were of poor quality at the same level. The comparison of the extra reconstructions in four patients with differing amounts of spokes found a decrease in sensitivity when the number of spokes was increased (21.4% for 144 spokes, 21.4% for 610 and 11.9% for 1345).

5.5 STUDY V

Results

MRI identified 12 patients with a positive PE and four patients were subsequently given anticoagulant treatment because of these findings. Thirteen patients who were suspected of having PE after clinical examination and then administered anticoagulants were found to

have a negative MRI and treatment thus suspended. A report of other finding was made, including effusion, consolidation, etc. One patient presented with a deep vein thrombosis (DVT) after a three-month checkup, and then had a stroke at 12 months, having presented with a negative MRI. Another patient also presented with a stroke but had a positive MRI. Eight patients died after three months and six within a year, but none of those patients died due to complications from DVT or PE. If a patient presented with a VTE in the EMR, together with a negative MRI, then the finding was considered a false negative. We obtained a sensitivity of 92.3% and a specificity of 100%.

6 DISCUSSION AND CONCLUSIONS

6.1 STUDY I

The study demonstrates that b-SSFP, used with 5 different slices at every position and with three orthogonal planes, has a good sensitivity and specificity. Neither breath holding nor cardiac triggering was included in our protocol, making the examination easy to perform. Two false negatives were reported in the study; both involving subsegmental embolism. It is known that MRI has difficulty in detecting small emboli in comparison to CTA, because of a lack in geometrical or temporal resolution. Twenty-nine of the 33 (88%) patients were positive, which is not representative of the normal distribution of PE cases; a figure of around 20% would be expected and this elevated distribution may have had an impact on the results.

Overall, the results found that b-SSFP using three different planes and 5 slices per position can be considered as an alternative in those patients that have a suspected PE but are contraindicated for CTA.

6.2 STUDY II

This study showed that DWI shows good sensitivity but suffers from poor specificity when detecting PE. The range of b values show different capabilities for detecting PE; for example, b 50 shows good sensitivity but an extremely poor specificity of 15%. The DWI sequence should not be used alone to investigate PE, however, it may be used as a supplementary technique when investigating other pathologies such as malignancies.

6.3 STUDY III

In this study, it was found that golden angle radial sampling schema produced images with a higher diagnostic quality than those made with Cartesian sampling. A good quality of image was also obtained when ECG was used; however, this may defeat the objective of the technique, as the b-SSFP protocol uses very short examination times, with speed of diagnosis being of benefit to the patient with suspect PE. An ECG triggered sequence will prolong the total examination time, the patient preparation and the scanning period.

6.4 STUDY IV

This study determined that the golden angle radial b-SSFP technique suffers from a low sensitivity and should not be used alone to depict acute PE. The aggregation of one or two more orthogonal planes to the protocol could be used to improve the detection of PE. In addition, the number of spokes used should be chosen carefully to achieve a good image

quality. The use of a reconstruction using spokes not contaminated with either respiratory or cardiac movements may help the efficacy of future studies.

6.5 STUDY V

This study reports the clinical outcome of 57 patients who were examined only with MRI due to a contraindication of CTA. No reference method was used. The data extracted from the EMR shows that there was one possible false negative. This patient presented with a DVT at the three-month control and then had a stroke within a year. We assume that all other negative MRI results not presenting with VTE in the EMR controls were true negatives, but without a reference method this is just speculation. We demonstrated that the MRI b-SSFP protocol can be used in the clinical management of patients presenting with a contraindication to CTA when treating PE.

7 ETHICAL CONSIDERATIONS

All studies included in this thesis were made in accordance with the Declaration of Helsinki (97), and were approved by the local ethics committee. All patients and volunteers were given written and verbal information on the study, and they were also interviewed with regards to the safety protocol, which included the MRI checklist to approve scanning in a magnetic field, according to the standard regulations of MRI safety at the hospital.

Each patient's treating physician was consulted to ascertain if they could be included in the study. No treatment was delayed due to the trial; most of the patients were already receiving treatment when they participated. In addition, there was no treatment delay when the study required that MRI was made prior to the standard examination, as it was performed in the period while the patient was waiting for the CTPA.

All patient and volunteer images were anonymized when presented to the radiologists. If a radiologist found some valuable clinical information when analyzing the images, this was reported to the patient's treating physician. In the volunteer group, the radiologists made findings in two people that were of clinical interest, however, neither of these lead to further investigations.

All patients and volunteers were examined using the standard hospital MRI scanner, with the corresponding standard technical regulation, following the MRI safety recommendation of both the hospital and international MRI safety guidelines (98, 99).

8 POINTS OF PERSPECTIVE

Several years have passed since the Prospective Investigation of Pulmonary Embolism Diagnose (PIOPED III) study (37), which compared magnetic resonance angiography to other techniques used to depict PE. In recent years, many investigators have tested the b-SSFP technique to diagnose PE and thus avoid the need to use intravenous contrast media, which is of benefit to those patients who are contraindicated. This type of sequence provides a fast image acquisition with a good contrast to noise ratio. Most of the previous studies use standard Cartesian sampling, which is sensitive to motion artefacts and so necessitates the use of a different technique to compensate or reduce the negative influence of motion from respiratory or cardiac movement. A respiratory compensation technique can be used, but this prolongs scan times. Alternatively, patients can be asked to hold their breath during the acquisition but in patients with suspected PE, they are often incapable of performing this maneuver. A shorter scan time can also be used when using the breath hold technique, however this results in a reduced image resolution. In recent years a new approach using radial sampling has become available which does not compromise in either resolution or scanning speed; the present study demonstrated that radial golden angle sampling is less sensitive to artefacts coming from flow or respiratory movements.

Currently there is no literature detailing use of the radial golden angle technique when investigating PE. Our protocol is based on the idea of repeating slices at the same position. This approach was demonstrated by Kluge et al. and in our own study, Nyrén et al. The effectiveness of having a choice of 5 slices placed at the same position suggests that “at least one of these should have good diagnostic quality”, as cited by the radiologists reviewing the images.

The radial golden angle post-reconstruction software allows the user to determine how many slices will be used per position. In our study, when using 144 spokes of a total of 1345, we obtained 21 different slices in every slice position. This is a huge increment in comparison to the 5 slices used in the Cartesian approach. However, the radiologists reported that the jumping phenomena between the slices was very distracting. This problem should be addressed when looking so many images with a short temporal resolution.

In order to obtain a high-quality image, we determined that the key factors are a short acquisition time, a good amount of signal to noise ratio, as few artefacts (movements, flow and striking) as possible, avoidance of jumping phenomena, and good contrast between blood and thrombi.

Future studies should be made with a software reconstruction algorithm that gives the radiologist the freedom to use the optimal temporal resolution as estimated for the individual patient, as individuals will have different patterns of respiratory movement. Selection of the number of spokes used is also key to quality; some images will have more clarity with under-sampling (144 spokes) while others will be better with over-sampling (144–1345). We should, perhaps, use a temporal resolution, depending on the patient's respiratory rate. In cardiac MRI studies, is possible to extract information from heart or respiratory movements from the total radial acquisition. This technique does not use spokes in the reconstruction of the images, which are contaminated with these movements and thus should give a better quality, or cleaner image. This flexibility in temporal resolution is one of the great advantages of the golden angle radial technique.

It would be of diagnostic benefit to the radiologist to scan in a different orthogonal plane, or alternatively the possibility of using radial golden angle 3D scanning could be investigated, as this would give radiologists the freedom to choose the plane needed. The continuing technical advancements of MRI will help to improve the quality of the images, for example, acceleration software that allows parallel imaging, such as Sensitivity Encoding (SENSE), Integrated Parallel Acquisition Technique (IPat), Generalized Auto-calibrating Partially Parallel Acquisition (GRAPPA) or Array Spatial Sensitivity Encoding Technique (ASSET). The development of new reconstruction software, for example Compressed Sensing, will help to improve the image, reducing the noise artefact. A valid question is whether software can help to improve in the speed of imaging with MRI. This is critical when scanning parts of the body that are in continual motion, such as the lungs and heart, and an increase in scanning speed should also improve the image quality in DWI; this technique requires the raw data to be processed quickly to obtain good images, good signal and little distortion.

New coil designs are also coming to the market; those which are soft and sheet-like allow the thorax to be surrounded, thus improving signal detection and this approach should be more comfortable for the patient due to the light weight. Other coils have longer elements to improve signal detection and allow the use of a higher acceleration factor when using SENSE or IPat or ASSET; this should increase the signal to noise ratio and reduce the scan time or increase the temporal resolution. Finally, greater cooperation between the manufacturing industry and clinicians would allow co-development of new tools to improve image quality, speed, diagnosis and patient comfort.

9 ACKNOWLEDGEMENTS

“Appreciation is a wonderful thing. It makes what is excellent in others belong to us as well.”-Voltaire

My appreciation and thankfulness for all the knowledge and invaluable time that I received from my supervisor and co-supervisors

To my supervisor Peter Lindholm, your time, your vision, your push, your energy has made this thesis possible. Thanks for trusting me. I know how much you have done.

To my co-supervisor Sven Nyrén, your time is gold, and you have been given me too much. Your patience has been unlimited, I hope it will never end. Thank you so much for all those days and evening working together.

To my co-supervisor Mikael Skorpil, you have been in the background waiting for me. Every time that I asked things you always presented a good answer. You have been the counter partner, no rush, thinking twice, thanks for everything

Veli Söderlund, so many years working together, an always so friendly. You have always time to listen, to talk, to sort out problems and give advices. Thanks for everything you have been giving me all these years.

To the best researchteam ever, tack till var och en, för allt hjälp, kunskap, råd och framför allt en mycket gott och okomplicerade samarbete, Alexander Fyrdahl, Koshiar Medson, Jimmy Yu, Anna Nordgren Rogberg,

Prof. Hans Ringertz, hoppas du har inte ångrat när du så ”ja, välkommen”, tack så jättemycket för en livs möjlighet Hans!

Prof. Lennart Blomqvist, du har alltid get mig uppmuntrande till utveckling och forskning, till att växa professionell, tack så mycket

Sofia Pettersson, alltid så enorm hjälpsam, tack för all din tid och tålamod med alla dessa frågor.

Eddie Weitzberg, hade hoppats att många kunde vara så positiva och okomplicerad som du.

Till alla mina chefer, under mina forskningsår, som har get mig chansen och tid att utvecklas, som har trott på mig.

Yords Österman, tack för allt du har lärt mig, för allt din tid, tack för att du är min arbetskollega som alltid finns.

Chikako Suzuki, tack för alla dessa kunskap givande och uppmuntrande samtal

Magnus Tengvar och Mikael Öberg, tack för alla dessa timmar som ni har jobbat med utvärdering.

Magnus Karlsson, tack för har alltid varit en god vän.

Mansour Haghgou, tack för allt din vänskap och uppmuntrande.

Andreas Carlberg, tack för allt din hjälp.

Kent Fridell och Jessika Ekberg, tack för ett bra samarbete och allt hjälp från er.

Till alla mina kollegor på MR som alltid uppmuntrat och stöttat mig mer eller mindre.

Tack till arbetsglädje som jag har haft med er.

Lars B., Hildur, Boel, Katarina, Ingmarie, Marie, Fatima, Jodit, Manijeh, Kirsi, Yvonne, Mansour, Hamid B., Mia, Maria, Fredrik, Csilla, Subhash, Maryam, Raheleh, Soheila, Thelma, Julia, Helen, Vanda, Fahimeh, Shervin, Håkon, Erik, Susanne, Ulrika, Abdulhamid, Tuija, Bibbi, Inger, Rezgar, Barwar, Zlatan, Asmaa, Hakeem, Bosse E., Kristofer, Evelina, Jasmin, Murtaza, Kirsi, Mimmi, Lennart L., Maggan, Calle, Mohammed

Till Sam, vi glömmer aldrig dig.

Tack till alla mina fina kollegor från södra sidan stan, Huddinge.

A mis colegas en Chile, Jose Miguel, Monica, Ana Maria, Magdalena, Julia, Alejandro, Carmen, Guillermo, Felipe, Veronica, Elisabeth, Maria Eugenia, Patricia, Noemi, Tato, Carla, Gerardo, Fernandez, Huete, Pefaur y Passalacqua.

A mis amigos en Chile de toda una vida, que siempre han estado cerca de mi, no necesito dar nombres.

Y al final lo mas importante de mi vida,

Mi familia, quien es uno sin una familia?

Gracias a mi amada familia, que siempre han estado conmigo, muy cerca y al mismo tiempo tan lejos.

Mis hijas, nietas(os), sus familias, sin ustedes nada funciona, nada tiene valor en mi vida si ustedes no estan presentes.

A mi madre Maria y mi padre Luis por todo los valores y esfuerzos que siempre me han dado.

A mis hermanas y hermanos, mis queridos sobrinos y sobrinas, gracias por todo el apoyo y carino incondicional que siempre he recivido.

10 REFERENCES

1. Calder**,** K., Herbert, M., & Henderson, S. (2005). The Mortality of Untreated Pulmonary Embolism in Emergency Department Patients. Annals of Emergency Medicine, 45(3), 302–310. https://doi.org/10.1016/j.annemergmed.2004.10.001

2. Egermayer, P., & Town, G. (1997). The clinical significance of pulmonary embolism: uncertainties and implications for treatment--a debate. Journal of Internal Medicine., 241(1), 5–10. https://doi.org/10.1046/j.1365-2796.1997.74880000.x

3. Beckman, M., Hooper, W., Critchley, S., & Ortel, T. (2010). Venous thromboembolism: a public health concern. American Journal of Preventive Medicine, 38(4 Suppl), S495–. https://doi.org/10.1016/j.amepre.2009.12.017

4. Heit, J., O'Fallon, W., Petterson, T., Lohse, C., Silverstein, M., Mohr, D., & Melton, L. (2002). Relative Impact of Risk Factors for Deep Vein Thrombosis and Pulmonary Embolism: A Population-Based Study. Archives of Internal Medicine (1960), 162(11), 1245–1248. https://doi.org/10.1001/archinte.162.11.1245

5. Walker, A., Card, T., West, J., Crooks, C., & Grainge, M. (2013). Incidence of venous thromboembolism in patients with cancer – A cohort study using linked United Kingdom databases. European Journal of Cancer (1990), 49(6), 1404–1413. https://doi.org/10.1016/j.ejca.2012.10.021

6. Carson, J., Kelley, M., Duff, A., Weg, J., Fulkerson, W., Palevsky, H., Schwartz, J., Thompson, B., Popovich, J., Hobbins, T., Spera, M., Alavi, A., & Terrin, M. (1992). The Clinical Course of Pulmonary Embolism. The New England Journal of Medicine, 326(19), 1240–1245. https://doi.org/10.1056/nejm199205073261902

7. Wagenvoort, C. (1995). Pathology of pulmonary thromboembolism. Chest., 107(1 Suppl), 10S–17S. https://doi.org/10.1378/chest.107.1_supplement.10s

8. Havig O. (1977). Deep vein thrombosis and pulmonary embolism: an autopsy study with multiple regression analysis of possible factors. Acta Chir Scand. 478(suppl):1-108

9. Moore, A., Wachsmann, J., Chamarthy, M., Panjikaran, L., Tanabe, Y., & Rajiah, P. (2018). Imaging of acute pulmonary embolism: an update. Cardiovascular Diagnosis and Therapy, 8(3), 225–243. https://doi.org/10.21037/cdt.2017.12.01

10. Wells P S., David R. Anderson, Marc Rodger, Ian Stiell, Jonathan F. Dreyer, David Barnes, Melissa Forgie, George Kovacs, John Ward, & Michael J. Kovacs. (2001). Excluding Pulmonary Embolism at the Bedside without Diagnostic Imaging: Management of Patients with Suspected Pulmonary Embolism Presenting to the Emergency Department by Using a Simple Clinical Model and d-dimer. Annals of Internal Medicine, 135(2), 98–. https://doi.org/10.7326/0003-4819-135-2-200107170-00010

11. Kluetz, P., & White, C. (2006). Acute Pulmonary Embolism: Imaging in the Emergency Department. The Radiologic Clinics of North America, 44(2), 259–271. https://doi.org/10.1016/j.rcl.2005.10.004

12. Goldhaber, S. Z., Visani, L., & De Rosa, M. (1999). Acute pulmonary embolism: clinical outcomes in the International Cooperative Pulmonary Embolism Registry (ICOPER). Lancet (London, England), 353(9162), 1386–1389. https://doi.org/10.1016/s0140-6736(98)07534-5

13. Righini, M., Robert-Ebadi, H., & Le Gal, G. (2017). Diagnosis of acute pulmonary embolism. Journal of Thrombosis and Haemostasis, 15(7), 1251–1261. https://doi.org/10.1111/jth.13694

14. Huisman, M., & Klok, F. (2013). Diagnostic management of acute deep vein thrombosis and pulmonary embolism. Journal of Thrombosis and Haemostasis, 11(3), 412–422. https://doi.org/10.1111/jth.12124

15. Abcarian, S. (2004). Role of a Quantitative D-Dimer Assay in Determining the Need for CT Angiography of Acute Pulmonary Embolism. American Journal of Roentgenology, 182(6), 1377–1381.

16. Ginsberg, W. (1998). Sensitivity and Specificity of a Rapid Whole-Blood Assay for D-Dimer in the Diagnosis of Pulmonary Embolism. Annals of Internal Medicine, 129(12), 1006–1011. https://doi.org/10.7326/0003-4819-129-12-199812150-00003

17. Bounameaux, D. (1997). D-dimer testing in suspected venous thromboembolism: an update. QJM : Monthly Journal of the Association of Physicians, 90(7), 437–442. https://doi.org/10.1093/qjmed/90.7.437

18. Wells, A. (2000). Derivation of a Simple Clinical Model to Categorize Patients Probability of Pulmonary Embolism: Increasing the Models Utility with the SimpliRED D-dimer. Thrombosis and Haemostasis, 83(3), 416–420. https://doi.org/10.1055/s-0037-1613830

19. Le Gal, R. (2006). Prediction of Pulmonary Embolism in the Emergency Department: The Revised Geneva Score. Annals of Internal Medicine, 144(3), 165–171. https://doi.org/10.7326/0003-4819-144-3-200602070-00004

20. Rahaghi, F., Minhas, J., & Heresi, G. (2018). Diagnosis of Deep Venous Thrombosis and Pulmonary Embolism: New Imaging Tools and Modalities. Clinics in Chest Medicine, 39(3), 493–.

21. Tapson, V. (2008). Acute Pulmonary Embolism. The New England Journal of Medicine, 358(10), 1037–1052. https://doi.org/10.1056/nejmra072753

22. Worsley, D., & Alavi, A. (1995). Comprehensive analysis of the results of the PIOPED Study. Prospective Investigation of Pulmonary Embolism Diagnosis Study. The Journal of Nuclear Medicine (1978), 36(12), 2380–.

23. Value of the Ventilation/Perfusion Scan in Acute Pulmonary Embolism: Results of the Prospective Investigation of Pulmonary Embolism Diagnosis **(PIOPED).** (1990). JAMA: the Journal of the American Medical Association, 263(20), 2753–2759. https://doi.org/10.1001/jama.1990.03440200057023

24. Sostman, H., Miniati, M., Gottschalk, A., Matta, F., Stein, P., & Pistolesi, M. (2008). Sensitivity and Specificity of Perfusion Scintigraphy Combined with Chest Radiography for Acute Pulmonary Embolism in PIOPED II. The Journal of Nuclear Medicine, 49(11), 1741–1748. https://doi.org/10.2967/jnumed.108.052217

25. Remy-Jardin, M., J Remy, L Wattinne, & F Giraud. (1992). Central pulmonary thromboembolism: diagnosis with spiral volumetric CT with the single-breath-hold technique--comparison with pulmonary angiography. Radiology, 185(2), 381–387. https://doi.org/10.1148/radiology.185.2.1410342

26. Remy-Jardin, M., Remy, J., Deschildre, F., Artaud, D., Beregi, J. P., Hossein-Foucher, C., Marchandise, X., & Duhamel, A. (1996). Diagnosis of pulmonary embolism with spiral CT: comparison with pulmonary angiography and scintigraphy. Radiology, 200(3), 699–706. https://doi.org/10.1148/radiology.200.3.8756918

27. Lomis, N. N., Yoon, H. C., Moran, A. G., & Miller, F. J. (1999). Clinical outcomes of patients after a negative spiral CT pulmonary arteriogram in the evaluation of acute pulmonary embolism. Journal of vascular and interventional radiology: JVIR, 10(6), 707–712. https://doi.org/10.1016/s1051-0443(99)70104-1

28. Perrier, A., Howarth, N., Didier, D., Loubeyre, P., Unger, P., de Moerloose, P., Slosman, D., Junod, A., & Bounameaux, H. (n.d.). Performance of helical computed tomography in unselected outpatients with suspected pulmonary embolism. Annals of Internal Medicine., 135(2), 88–97. https://doi.org/10.7326/0003-4819-135-2-200107170-00008

29. Remy-Jardin, M., Mastora, I., & Remy, J. (2003). Pulmonary embolus imaging with multislice CT. Radiologic clinics of North America, 41(3), 507–519. https://doi.org/10.1016/s0033-8389(03)00028-9

30. Konstantinides, S., Meyer, G., Becattini, C., Bueno, H., Geersing, G., Harjola, V., Huisman, M., Humbert, M., Jennings, C., Jiménez, D., Kucher, N., Lang, I., Lankeit, M., Lorusso, R., Mazzolai, L., Meneveau, N., Áinle, F., Prandoni, P., Pruszczyk, P., … Torbicki, A. (2019). **2019 ESC Guidelines** for the diagnosis and management of acute pulmonary embolism developed in collaboration with the European Respiratory Society (ERS): The Task Force for the diagnosis and management of acute pulmonary embolism of the European Society of Cardiology (ESC). European Respiratory Journal., 54(3). https://doi.org/10.1183/13993003.01647-2019

31. Coresh, J., Astor, B., Greene, T., Eknoyan, G., & Levey, A. (2003). Prevalence of chronic kidney disease and decreased kidney function in the adult US population: Third national health and nutrition examination survey. American Journal of Kidney Diseases, 41(1), 1–12. https://doi.org/10.1053/ajkd.2003.50007

32. Edelman, R., Silvers, R., Thakrar, K., Metzl, M., Nazari, J., Giri, S., & Koktzoglou, I. (2017). Nonenhanced MR angiography of the pulmonary arteries using single-shot radial quiescent-interval slice-selective (QISS): a technical feasibility study. Journal of Cardiovascular Magnetic Resonance, 19(1), 48–8. https://doi.org/10.1186/s12968-017-0365-3

33. Stein, P., Fowler, S., Goodman, L., Gottschalk, A., Hales, C., Hull, R., Leeper, K., Popovich, J., Quinn, D., Sos, T., Sostman, H., Tapson, V., Wakefield, T., Weg, J., & Woodard, P. (2006). Multidetector Computed Tomography for Acute Pulmonary Embolism. The New England Journal of Medicine, 354(22), 2317–2327. https://doi.org/10.1056/nejmoa052367

34. Ohno, Y., Yoshikawa, T., Kishida, Y., Seki, S., & Karabulut, N. (2017). Unenhanced and Contrast-Enhanced MR Angiography and Perfusion Imaging for Suspected Pulmonary Thromboembolism. AJR. American journal of roentgenology, 208(3), 517–530. https://doi-org.proxy.kib.ki.se/10.2214/AJR.16.17415

35. Kanne, J. P., & Lalani, T. A. (2004). Role of computed tomography and magnetic resonance imaging for deep venous thrombosis and pulmonary embolism. Circulation, 109(12 Suppl 1), I15–I21. https://doi-org.proxy.kib.ki.se/10.1161/01.CIR.0000122871.86662.72

36. Prince, M. (1994). Gadolinium-enhanced MR aortography. Radiology, 191(1), 155–164. https://doi.org/10.1148/radiology.191.1.8134563

37. Stein, P. (2010). Gadolinium-Enhanced Magnetic Resonance Angiography for Pulmonary Embolism: A Multicenter Prospective Study (PIOPED III). Annals of Internal Medicine, 152(7), 434–. https://doi.org/10.7326/0003-4819-152-7-201004060-00008

38. Grenier, P., & Beigelman, C. (1998). Spiral computed tomographic scanning and magnetic resonance angiography for the diagnosis of pulmonary embolism. Thorax, 53(suppl 2), S25–S31. https://doi.org/10.1136/thx.53.2008.S25

39. Revel, M., Sanchez, O., Couchon, S., Planquette, B., Hernigou, A., Niarra, R., Meyer, G., & Chatellier, G. (2012). Diagnostic accuracy of magnetic resonance imaging for an acute pulmonary embolism: results of the "IRM-EP" study. Journal of Thrombosis and Haemostasis, 10(5), 743–750. https://doi.org/10.1111/j.1538-7836.2012.04652.x

40. Revel, M. P., Sanchez, O., Lefort, C., Meyer, G., Couchon, S., Hernigou, A., Niarra, R., Chatellier, G., & Frija, G. (2013). Diagnostic accuracy of unenhanced, contrast-enhanced perfusion and angiographic MRI sequences for pulmonary embolism diagnosis: results of independent sequence readings. European radiology, 23(9), 2374–2382. https://doi-org.proxy.kib.ki.se/10.1007/s00330-013-2852-8

41. Kalb, B., Sharma, P., Tigges, S., Ray, G., Kitajima, H., Costello, J., Chen, Z., & Martin, D. (2012). MR Imaging of Pulmonary Embolism: Diagnostic Accuracy of Contrast-enhanced 3D MR Pulmonary Angiography, Contrast-enhanced Low–Flip Angle 3D GRE, and Nonenhanced Free-Induction FISP Sequences. Radiology, 263(1), 271–278. https://doi.org/10.1148/radiol.12110224

42. Nagle, S., Schiebler, M., Repplinger, M., François, C., Vigen, K., Yarlagadda, R., Grist, T., & Reeder, S. (2016). Contrast enhanced pulmonary magnetic resonance angiography for pulmonary embolism: Building a successful program. European Journal of Radiology, 85(3), 553–563. https://doi.org/10.1016/j.ejrad.2015.12.018

43. Ingrisch, M., Maxien, D., Meinel, F., Reiser, M., Nikolaou, K., & Dietrich, O. (2016). Detection of pulmonary embolism with free-breathing dynamic contrast-enhanced MRI. Journal of Magnetic Resonance Imaging, 43(4), 887–893. https://doi.org/10.1002/jmri.25050

44. Maxien, D., Ingrisch, M., Meinel, F., Reiser, M., Dietrich, O., & Nikolaou, K. (2013). Quantification of Pulmonary Perfusion with Free-Breathing Dynamic Contrast-Enhanced MRI – A Pilot Study in Healthy Volunteers. RöFo - Fortschritte Auf Dem Gebiet Der Röntgenstrahlen Und Der Bildgebenden Verfahren, 185(12), 1175–1181. https://doi.org/10.1055/s-0033-1350128

45. Ramalho, J., Ramalho, M., Jay, M., Burke, L., & Semelka, R. (2016). Gadolinium toxicity and treatment. Magnetic Resonance Imaging, 34(10), 1394–1398. https://doi.org/10.1016/j.mri.2016.09.005

46. Thomsen, H. (2006). Nephrogenic systemic fibrosis: a serious late adverse reaction to gadodiamide. European Radiology, 16(12), 2619–2621. https://doi.org/10.1007/s00330-006-0495-8

47. Fraum, T., Ludwig, D., Bashir, M., & Fowler, K. (2017). Gadolinium-based contrast agents: A comprehensive risk assessment. Journal of Magnetic Resonance Imaging, 46(2), 338–353. https://doi.org/10.1002/jmri.25625

48. Semelka, R., Ramalho, M., AlObaidy, M., & Ramalho, J. (2016). Gadolinium in Humans: A Family of Disorders. American Journal of Roentgenology (1976), 207(2), 229–233. https://doi.org/10.2214/AJR.15.15842

49. Gulani, V., Calamante, F., Shellock, F., Kanal, E., & Reeder, S. (2017). Gadolinium deposition in the brain: summary of evidence and recommendations. Lancet Neurology, 16(7), 564–570. https://doi.org/10.1016/S1474-4422(17)30158-8

50. Eklöf, H., Smedby, O., Ljungman, C., Karacagil, S., Bergqvist, D., & Ahlström, H. (1998). 2D inflow MR angiography in severe chronic leg ischemia. Acta radiologica (Stockholm, Sweden: 1987), 39(6), 663–668. https://doi-org.proxy.kib.ki.se/10.3109/02841859809175493

51. Leiner, T. (2005). Magnetic resonance angiography of abdominal and lower extremity vasculature. Topics in Magnetic Resonance Imaging, 16(1), 21–66. https://doi.org/10.1097/01.rmr.0000185431.50535.d7

52. Miyazaki, M., & Akahane, M. (2012). Non-contrast enhanced MR angiography: Established techniques. Journal of Magnetic Resonance Imaging, 35(1), 1–19. https://doi.org/10.1002/jmri.22789

53. Okuaki, T., Ishimoto, T., Miyati, T., Kobayashi, S., Ishihara, M., Kawakami, M., Ogino, T., & Van Cauteren, M. (2014). Separate pulmonary artery and vein magnetic resonance angiography by use of an arterial spin labeling method. Radiological Physics and Technology, 7(2), 352–357. https://doi.org/10.1007/s12194-014-0272-3

54. Andia, M., & Botnar, R. (2012). Arterial spin labeling angiography using a triple inversion recovery prepulse. Magnetic Resonance in Medicine, 67(2), 477–483. https://doi.org/10.1002/mrm.23028

55. Shin, T., Worters, P., Hu, B., & Nishimura, D. (2013). Non-contrast-enhanced renal and abdominal MR angiography using velocity-selective inversion preparation. Magnetic Resonance in Medicine, 69(5), 1268–1275. https://doi.org/10.1002/mrm.24356

56. Scheffler, K., & Lehnhardt, S. (2003). Principles and applications of balanced SSFP techniques. European Radiology, 13(11), 2409–2418. https://doi.org/10.1007/s00330-003-1957-x

57. Bieri**,** O., & Scheffler, K. (2013). Fundamentals of balanced steady state free precession MRI. Journal of magnetic resonance imaging: JMRI, *38*(1), 2–11. https://doi-org.proxy.kib.ki.se/10.1002/jmri.24163

58. Schieda, N., Isupov, I., Chung, A., Coffey, N., & Avruch, L. (2017). Practical applications of balanced steady-state free-precession (bSSFP) imaging in the abdomen and pelvis. Journal of Magnetic Resonance Imaging, 45(1), 11–20. https://doi.org/10.1002/jmri.25336

59. Heye, T., Sommer, G., Miedinger, D., Bremerich, J., & Bieri, O. (2015). Ultrafast 3D balanced steady-state free precession MRI of the lung: Assessment of anatomic details in comparison to low-dose CT: Ultrafast 3D bSSFP MRI of the Lung. Journal of Magnetic Resonance Imaging, 42(3), 602–609. https://doi.org/10.1002/jmri.24836

60. Herédia, V., Altun, E., Ramalho, M., de Campos, R., Azevedo, R., Pamuklar, E., & Semelka, R. C. (2012). MRI of pregnant patients for suspected pulmonary embolism: steady-state free precession vs postgadolinium 3D-GRE. Acta medica portuguesa, *25*(6), 359–367.

61. Kaya, F., Ufuk, F., & Karabulut, N. (2019). Diagnostic performance of contrast-enhanced and unenhanced combined pulmonary artery MRI and magnetic resonance venography techniques in the diagnosis of venous thromboembolism. The British journal of radiology, 92(1095), 20180695. https://doi-org.proxy.kib.ki.se/10.1259/bjr.20180695

62. Nyrén, S., Nordgren Rogberg, A., Vargas Paris, R., Bengtsson, B., Westerlund, E., & Lindholm, P. (2017). Detection of pulmonary embolism using repeated MRI acquisitions without respiratory gating: a preliminary study. Acta Radiologica (1987), 58(3), 272–278. https://doi.org/10.1177/0284185116651003

63. Kluge, A., Müller, C., Hansel, J., Gerriets, T., & Bachmann, G. (2004). Real-time MR with TrueFISP for the detection of acute pulmonary embolism: initial clinical experience. European Radiology, 14(4), 709–718. https://doi.org/10.1007/s00330-003-2164-5

64. Kluge, A., Luboldt, W., & Bachmann, G. (2006). Acute Pulmonary Embolism to the Subsegmental Level: Diagnostic Accuracy of Three MRI Techniques Compared with 16-MDCT. American Journal of Roentgenology (1976), 187(1), W7–W14. https://doi.org/10.2214/ajr.04.1814

65. Le Bihan, D., Mangin, J. F., Poupon, C., Clark, C. A., Pappata, S., Molko, N., & Chabriat, H. (2001). Diffusion tensor imaging: concepts and applications. Journal of magnetic resonance imaging: JMRI, 13(4), 534–546. https://doi-org.proxy.kib.ki.se/10.1002/jmri.1076

66. Rosenkrantz, A., Padhani, A., Chenevert, T., Koh, D., De Keyzer, F., Taouli, B., & Le Bihan, D. (2015). Body diffusion kurtosis imaging: Basic principles, applications, and considerations for clinical practice. Journal of Magnetic Resonance Imaging, 42(5), 1190–1202. https://doi.org/10.1002/jmri.24985

67. Dietrich, O., Biffar, A., Baur-Melnyk, A., & Reiser, M. (2010). Technical aspects of MR diffusion imaging of the body. European Journal of Radiology, 76(3), 314–322. https://doi.org/10.1016/j.ejrad.2010.02.018

68. Pruessmann, K., Weiger, M., Börnert, P., & Boesiger, P. (2001). Advances in sensitivity encoding with arbitrary k -space trajectories. Magnetic Resonance in Medicine, 46(4), 638–651. https://doi.org/10.1002/mrm.1241

69. Iima, M., & Le Bihan, D. (2016). Clinical Intravoxel Incoherent Motion and Diffusion MR Imaging: Past, Present, and Future. Radiology, 278(1), 13–32. https://doi.org/10.1148/radiol.2015150244

70. Koh, D., & Collins, D. (2007). Diffusion-Weighted MRI in the Body: Applications and Challenges in Oncology. American Journal of Roentgenology (1976), 188(6), 1622–1635. https://doi.org/10.2214/ajr.06.1403

71. O. Stejskal and J. E. Tanner. (1965). Spin Diffusion Measurements: Spin Echos in the Presence of a Time-Dependent Field Gradient. The Journal of Chemical Phisics 42:1, 288-292 https://doi.org/10.1063/1.1695690

72. Bammer, R. (2003). Basic principles of diffusion-weighted imaging. European Journal of Radiology, 45(3), 169–184. https://doi.org/10.1016/s0720-048x(02)00303-0

73. Eiber, M., Holzapfel, K., Ganter, C., Epple, K., Metz, S., Geinitz, H., Kübler, H., Gaa, J., Rummeny, E., & Beer, A. (2011). Whole-body MRI including diffusion-weighted imaging (DWI) for patients with recurring prostate cancer: Technical feasibility and assessment of lesion conspicuity in DWI. Journal of Magnetic Resonance Imaging, 33(5), 1160–1170. https://doi.org/10.1002/jmri.22542

74. Stecco, A., Buemi, F., Iannessi, A., Carriero, A., & Gallamini, A. (2018). Current concepts in tumor imaging with whole-body MRI with diffusion imaging (WB-MRI-DWI) in multiple myeloma and lymphoma. Leukemia & Lymphoma, 59(11), 2546–2556. https://doi.org/10.1080/10428194.2018.1434881

75. Meier-Schroers, M., Homsi, R., Skowasch, D., Buermann, J., Zipfel, M., Schild, H., & Thomas, D. (2018). Lung cancer screening with MRI: results of the first screening round. Journal of Cancer Research and Clinical Oncology, 144(1), 117–125. https://doi.org/10.1007/s00432-017-2521-4

76. Sandrasegaran, K., Tahir, B., Nutakki, K., Akisik, F., Bodanapally, U., Tann, M., & Chalasani, N. (2013). Usefulness of conventional MRI sequences and diffusion-weighted imaging in differentiating malignant from benign portal vein thrombus in cirrhotic patients. American Journal of Roentgenology (1976), 201(6), 1211–1219. https://doi.org/10.2214/AJR.12.10171

77. Catalano, O., Choy, G., Zhu, A., Hahn, P., & Sahani, D. (2010). Differentiation of Malignant Thrombus from Bland Thrombus of the Portal Vein in Patients with Hepatocellular Carcinoma: Application of Diffusion-weighted MR Imaging. Radiology, 254(1), 154–162. https://doi.org/10.1148/radiol.09090304

78. Ahn, J., Yu, J., Cho, E., Chung, J., Kim, J., & Kim, K. (2016). Diffusion-Weighted MRI of Malignant versus Benign Portal Vein Thrombosis. Korean Journal of Radiology, 17(4), 533–540. https://doi.org/10.3348/kjr.2016.17.4.533

79. Lustig, M., Donoho, D., & Pauly, J. (2007). Sparse MRI: The application of compressed sensing for rapid MR imaging. Magnetic Resonance in Medicine, 58(6), 1182–1195. https://doi.org/10.1002/mrm.21391

80. Pipe JG, Motion correction with PROPELLER MRI: application to head motion and free-breathing cardiac imaging.
Magn Reson Med. 1999 Nov;42(5):963-9

81. Runge V M, J A Clanton, C L Partain, & A E James, J. (1984). Respiratory gating in magnetic resonance imaging at 0.5 Tesla. Radiology, 151(2), 521–523. https://doi.org/10.1148/radiology.151.2.6709928

82. Glover GH, Pauly JM. Projection reconstruction techniques for reduction of motion effects in MRI. Magn Reson Med. 1992 Dec;28(2):275-89.

83. Hirokawa, Y., Isoda, H., Maetani, Y., Arizono, S., Shimada, K., & Togashi, K. (2008). Evaluation of motion correction effect and image quality with the periodically rotated overlapping parallel lines with enhanced reconstruction (PROPELLER) (BLADE) and parallel imaging acquisition technique in the upper abdomen. Journal of Magnetic Resonance Imaging, 28(4), 957–962. https://doi.org/10.1002/jmri.21538

84. Feng, L., Benkert, T., Block, K., Sodickson, D., Otazo, R., & Chandarana, H. (2017). Compressed sensing for body MRI. Journal of Magnetic Resonance Imaging, 45(4), 966–987. https://doi.org/10.1002/jmri.25547

85. Rasche, V., Boer, R., Holz, D., & Proksa, R. (1995). Continuous radial data acquisition for dynamic MRI. Magnetic Resonance in Medicine, 34(5), 754–761. https://doi.org/10.1002/mrm.1910340515

86. Azevedo, d. (2011). Free-breathing 3D T1-weighted gradient-echo sequence with radial data sampling in abdominal MRI: preliminary observations. American Journal of Roentgenology (1976), 197(3), 650–657. https://doi.org/10.2214/AJR.10.5881

87. Winkelmann, S., Schaeffter, T., Koehler, T., Eggers, H., & Doessel, O. (2007). An optimal radial profile order based on the Golden Ratio for time-resolved MRI. IEEE Trans Med Imaging, 26(1), 68–76. https://doi.org/10.1109/TMI.2006.885337

88. Feng, G. (2014). Golden-angle radial sparse parallel MRI: Combination of compressed sensing, parallel imaging, and golden-angle radial sampling for fast and flexible dynamic volumetric MRI. Magnetic Resonance in Medicine, 72(3), 707–717. https://doi.org/10.1002/mrm.24980

89. Demerath, B. (2020). Golden-Angle Radial Sparse Parallel (GRASP) MRI differentiates head & neck paragangliomas from schwannomas. Magnetic Resonance Imaging, 70, 73–80. https://doi.org/10.1016/j.mri.2020.04.003

90. Stroud, R., Piccini, D., Schoepf, U., Heerfordt, J., Yerly, J., Di Sopra, L., Rollins, J., Fischer, A., Suranyi, P., & Varga-Szemes, A. (2019). Correcting versus resolving respiratory motion in free-breathing whole-heart MRA: a comparison in patients with thoracic aortic disease. European Radiology Experimental, 3(1), 1–8. https://doi.org/10.1186/s41747-019-0107-4

91. Piccini, D., Feng, L., Bonanno, G., Coppo, S., Yerly, J., Lim, R., Schwitter, J., Sodickson, D., Otazo, R., & Stuber, M. (2017). Four-dimensional respiratory motion-resolved whole heart coronary MR angiography. Magnetic Resonance in Medicine, 77(4), 1473–1484. https://doi.org/10.1002/mrm.26221

92. Feng, L., Delacoste, J., Smith, D., Weissbrot, J., Flagg, E., Moore, W., Girvin, F., Raad, R., Bhattacharji, P., Stoffel, D., Piccini, D., Stuber, M., Sodickson, D., Otazo, R., & Chandarana, H. (2019). Simultaneous Evaluation of Lung Anatomy and Ventilation Using 4D Respiratory-Motion-Resolved Ultrashort Echo Time Sparse MRI. Journal of Magnetic Resonance Imaging, 49(2), 411–422. https://doi.org/10.1002/jmri.26245

93. Li, L. (2018). Feasibility of free-breathing dynamic contrast-enhanced MRI of gastric cancer using a golden-angle radial stack-of-stars VIBE sequence: comparison with the conventional contrast-enhanced breath-hold 3D VIBE sequence. European Radiology, 28(5), 1891–1899. https://doi.org/10.1007/s00330-017-5193-1

94. Lin, W., Guo, J., Rosen, M., & Song, H. (2008). Respiratory motion-compensated radial dynamic contrast-enhanced (DCE)-MRI of chest and abdominal lesions. Magnetic Resonance in Medicine, 60(5), 1135–1146. https://doi.org/10.1002/mrm.21740

95. Chen, L. (2018). Free-breathing dynamic contrast-enhanced MRI for assessment of pulmonary lesions using golden-angle radial sparse parallel imaging. Journal of Magnetic Resonance Imaging, 48(2), 459–468. https://doi.org/10.1002/jmri.25977

96. Sengupta, S. (2015). Continuously moving table MRI with golden angle radial sampling: CMT MRI with Golden Angle Radial Sampling. Magnetic Resonance in Medicine, 74(6), 1690–1697. https://doi.org/10.1002/mrm.25531

97. World Medical Association Declaration of Helsinki: Ethical Principles for Medical Research Involving Human Subjects. (2013). JAMA: The Journal of the American Medical Association, 310(20), 2191–2194. https://doi.org/10.1001/jama.2013.281053

98. Kanal, B. (2007). ACR Guidance Document for Safe MR Practices: 2007. American Journal of Roentgenology (1976), 188(6), 1447–1474. https://doi.org/10.2214/ajr.06.1616

99. Greenberg, H. (2019). ACR guidance document on MR safe practices: Updates and critical information 2019. Journal of Magnetic Resonance Imaging, 51(2), 331–338. https://doi.org/10.1002/jmri.26880